Eur. J. Mineral., 37, 793–817, 2025 https://doi.org/10.5194/ejm-37-793-2025 © Author(s) 2025. This work is distributed under the Creative Commons Attribution 4.0 License.





Changing magma dynamics and plumbing system architecture at an explosive—effusive transition: the case of Nisyros volcano (Greece)

Eleonora Braschi¹, Francesca Giannetti², Filippo Mastroianni², Andrea Orlando¹, Riccardo Avanzinelli², Simone Tommasini^{1,2}, Georges Enea Vougioukalakis³, and Lorella Francalanci²

¹Istituto di Geoscienze e Georisorse, Unità secondaria di Firenze, Consiglio Nazionale delle Ricerche, Via G. La Pira 4, 50121, Firenze, Italy

²Dipartimento di Scienze della Terra, Università degli Studi di Firenze, Via G. La Pira 4, 50141, Florence, Italy ³Department of Natural & Technological Hazards, Hellenic Survey of Geology and Mineral Exploration, S. Lui 1, Olympic Village, 13677 Aharne, Athens, Greece

Correspondence: Eleonora Braschi (eleonora.braschi@igg.cnr.it)

Received: 28 February 2025 - Revised: 3 July 2025 - Accepted: 21 July 2025 - Published: 22 October 2025

Abstract. Multiple magma storage levels are commonly recognized beneath magmatic systems and may play an important role in the processes leading to the build-up of large silicic magma chambers in the crust, with possible critical implications for the occurrence of explosive eruptions. Within such reservoirs, interactions between different magmas due to new recharge events are common processes, as demonstrated by the presence of mafic enclaves, which also reveal the occurrence of magma immiscibility conditions.

In Nisyros (Greece), the two most recent eruptive events are the caldera-forming explosive eruption of the Upper Pumice (UP) and the following effusive activity of the Post Caldera Domes (PCD), which emplaced a thick pyroclastic deposit and six main lava domes, both hosting mafic components as crystal-rich clasts (CRCs) and enclaves, respectively. These two eruptions show differences in the abundance, petrographic characteristics, mineral chemistry, and geochemical and isotopic signatures of their mafic components, as well as in the extent of their mingling processes, indicating that the magma interaction conditions were different, possibly related to a change in the magma chamber dynamics and/or in the deeper feeding system structure.

In this work, we investigated the textural characteristics and mineral chemistry of the products erupted by these two eruptive episodes, exploring their crystallization histories and the possible variations in physical conditions to reconstruct the structure of the plumbing system throughout the two phases of activities. Our results revealed the occurrence of evident mineral disequilibria within CRCs and enclaves related to their rapid crystallization due to the undercooling within the host. In the PCD systems, mineral disequilibria are also related to the extensive crystal transfer from the host to the enclaves and vice versa, generating mingling at the microscale, which increases with time. The application of geothermobarometers records progressively higher pressure from the UP to the PCD under similar temperature conditions. This indicates a deepening of the main eruptible reservoir, sampled by the PCD activity, after the UP–caldera collapse. Between the two periods, an interconnected evolved magma-rich system developed through new inputs of mafic melts that refilled and reheated the system, progressively mingling with the host and generating new conditions for the eruption.

1 Introduction

The presence of multiple magma storage levels is a common feature of magmatic systems, and it has been interpreted as being related to the complex processes leading to the formation of large silicic magma chambers in the crust (i.e., Sparks et al., 2024; Sparks et al., 2022; Cashman et al., 2017; Cashman and Giordano, 2014).

The identification of different ponding levels and their evolution, interconnection, possible reactivation, or vanishing over time represents a challenge for the understanding of feeding system dynamics and architecture, with fundamental implications for volcanic eruptions as well. Modern interpretations of volcanic plumbing systems suppose that magma generation, storage, and differentiation take place within vertically extensive mush reservoirs, where residual melts are distributed and segregated into (eruptible) melt-rich regions (Sparks et al., 2022). In this view, zoned trans-crustal magma systems are formed by progressive separation from basaltic magmas stored within lower crustal hot zones. Differentiation occurs mostly in the lower and middle crust, with the upper crustal levels predominantly characterized by magma accumulation and segregation (i.e., Annen et al., 2006; Cashman et al., 2017; Sparks et al., 2022, 2024).

However, it is unquestionable that magmas (magma chambers or melt zones within mush reservoirs) behave as open systems, as supported by evidence from both magma (i.e., whole-rock) chemistry and crystal records (i.e., crystal zoning) (e.g., DePaolo, 1981; Francalanci et al., 2005; Browne et al., 2006; Davidson et al., 2007; Ruprecht and Wörner, 2007; Petrone et al., 2018). Magma mingling, expressed by the presence of two or more chemically distinct magmas (i.e., Bacon and Metz, 1984), provides an important piece of evidence that magma chambers are assembled by episodic magma addition from below. Magma recharge episodes of mafic, hotter melts from depths represents, together with volatile accumulation, one of the principal factors that may trigger volcanic eruptions, producing a perturbation in the shallower portions of a plumbing system (i.e., Ruprecht et al., 2020). Thermal and physical interactions between differently evolved magmas are thus important processes that may rejuvenate the whole feeding system, potentially generating the conditions for explosive eruptions (Di Salvo et al., 2020; Forni et al., 2016). These recharge events may produce mixing; when magmas are very different in terms of temperature, composition, crystal content, and volatile content (and thus viscosity), immiscibility processes (mingling) may be favored instead, resulting in banded structures or enclaves (e.g., Bacon, 1986; Huppert, 1989; Laumonier et al., 2014; Blake and Fink, 2000; Coombs et al., 2002; Ruprecht et al., 2020). In general, enclaves are formed by more primitive magmas with respect to the host and are often interpreted as evidence of recharge events that trigger volcanic eruptions. However, they may also form during recharge episodes without the occurrence of eruptions, feeding and sustaining the

magma chamber (Ruprecht et al., 2020). In any case, enclaves are evidence of a dynamic system in which different magmas coexist in the same reservoir for an undefined period before eruption and are eventually emplaced together.

Such magma interactions may develop from macro- to microscale, through disaggregation of one (or more) components into the host (i.e., Humphreys et al., 2009; Braschi et al., 2012, 2014), with separation and dispersion of single mineral phases as well, resulting in disequilibrium paragenesis with respect to the host melt.

The possibility of detailing the dynamics of magma interaction and defining the physical conditions, such as pressure and temperature, as well as their possible variation over time and between different eruptions, represents an important step forward in the knowledge of magmatic systems. Mineral chemistry investigations are the principal tools for tracing such processes since crystals provide records of the processes occurring in the magmatic system in which they grew. Chemico-physical variations or episodic perturbations in a magmatic system are indeed recorded in the distinct compositions and zonings of crystallizing mineral phases, allowing the history of magma evolution to be tracked. Moreover, mineral composition can be used, through geothermobarometers, to constrain the depths and temperatures of magma storage and thus the structure and extent of the plumbing system. In this field, new machine learning algorithms have recently been proposed (i.e., Petrelli et al., 2020; Higgins et al., 2022; Chicchi et al., 2023) as an alternative to classical thermodynamic-based tools, which require equilibrium boundary conditions (i.e., Putirka, 2016, 2008) that are often hard to attain in open systems as volcanic magma chambers.

Nisyros volcano (Greece) shows evidence of mingling/mixing processes during its volcanological evolution and represents an excellent example to explore the relationship among magmas and reconstruct the deep-to-shallow structure of the feeding plumbing system. This volcano is also characterized by a shift in its eruptive style during the final magmatic history, changing from explosive, calderaforming eruptions to effusive phases emplacing large volumes of lava domes rich in mafic enclaves (Braschi et al., 2012, 2022).

In this paper we present new, detailed microanalytical data on the main mineral phases present in the different juvenile components erupted by these two different activities with the following aims:

- 1. to detail the interaction processes that characterize the different magmas before the eruption
- 2. to define the plumbing system architecture in terms of depth and thermal conditions of the different storage levels in order to determine if and how these conditions change from the final caldera-forming explosive stage to the effusive phase.

2 Geological and petrological background

The volcano of Nisyros is located in the easternmost sector of the South Aegean Active Volcanic Arc (SAAVA) and is part of the Kos–Nisyros volcanic field. The subaerial activity is younger than the 161 ka Kos Plateau tuff eruption of the nearby Kos volcano (Bachmann et al., 2007; Smith et al., 1996). The volcanic edifice grew on a basement of Mesozoic limestone and Neogene sediments (Barberi et al., 1988; Varekamp, 1993; Volentik et al., 2002) through two different cycles of activity, forming the present-day composite volcano, which is characterized by a large central caldera depression (about 4 km wide; Fig. 1).

The first cycle (< 161–47 ka; Bachmann et al., 2007; Margari et al., 2007) led to the formation of the volcanic edifice through the emission of lava flows and pyroclastic products, with effusive and mild explosive activity. The second cycle (ca. 47–19.9 ka; Margari et al., 2007; Popa et al., 2020) was marked by two Plinian or sub-Plinian caldera-forming explosive eruptions (Lower Pumice and Upper Pumice – Fig. 2a–c, respectively), emplacing thick deposits of pyroclastic material, both followed by abundant emission of lava flows and domes rich in magmatic enclaves (Nikia and Post Caldera Domes and lavas – Fig. 2d–f) (Davis, 1967; Di Paola, 1974; Wyers and Barton, 1989; Limburg and Varekamp, 1991; Seymour and Vlassopoulos, 1992; Francalanci et al., 1995; Volentik et al., 2005; Buettner et al., 2005; Vanderkluysen et al., 2005; Longchamp et al., 2011; Braschi et al., 2012; Klaver et al., 2017; Dietrich, 2018). The Post Caldera Domes activity emplaced six main lava domes in temporal succession. Historic phreatic explosions are documented in 1871-1873 and 1887 CE, testifying to a system that is still active and releasing heat from depth.

From the first to the second cycle of activity, the volcanic behavior and the compositional characteristics of the erupted magmas changed significantly. The products that erupted in the first cycle show a variable degree of differentiation from basaltic andesites to dacites, with rare rhyolites, alternatively emplaced during distinct eruptive events, thus defining recurrent jumps in the degree of evolution along the stratigraphic series (Francalanci et al., 1995). In contrast, the products that erupted during the second cycle of activity display evident bimodal compositions with large volumes of highly differentiated magmas (rhyolites and rhyodacites) emplaced together with variable amounts of mafic magmatic enclaves (from basalts and basaltic andesites to andesites) (Francalanci et al., 1995; Braschi et al., 2012; Klaver et al., 2017, 2018). In general, the observed large variability through time in the porphyritic index of the volcanic products and its correlation with the Sr isotope ratios has led researchers to propose complex magma evolutionary processes for Nisyros magmas, occurring within a stable, long-lived magma chamber undergoing multiple inputs and several cycles of crystal retentions, convections, and buoyancy-driven melt segregation (Francalanci et al., 1995). More recently, other authors have suggested the occurrence of two distinct magmatic suites (low-porphyritic andesite and high-porphyritic rhyodacite suites), which are considered to have evolved along distinct petrogenetic pathways through time (Klaver et al., 2017, 2018). However, the peculiar characteristics of the volcanic products erupted during the second cycle of activity suggest the establishment of a dynamic plumbing system dominated by multiple episodes of refilling/refreshing of an evolved magma chamber by mafic magmas, generating marked magma immiscibility (Francalanci et al., 1995; Braschi et al., 2012) and testifying to periodic recharges of the shallow system from below.

This is well documented in the products of the last two eruptions: the caldera-forming explosive eruption of the rhyolitic Upper Pumice (UP), emplaced as a thick pumice-rich pyroclastic deposit, and the following effusive activity of the rhyodacitic Post Caldera Domes (PCD). Both these activities are rich in mafic components that can be defined as mafic crystal-rich clasts (CRCs) in the UP and magmatic enclaves in the PCD (Braschi et al., 2012, 2022) (Fig. 2b-c, e-f). The age of these two events is constrained at 46.8 ± 5.7 ka (Margari et al., 2007) and 58.4 ± 2.7 ka (Popa et al., 2020) for the UP, based on a ¹⁴C core sample and U/Th on zircon, respectively, whereas the age of the PCD has been inferred on the basis of field observations to be in the range of 31–10 ka (see Braschi et al., 2012). New zircon U/Th dating by Locher et al. (2025) confirms the previous estimates, constraining the dome crystallization between 26 and 13 ka. This suggests a significant period of quiescence in the magmatic activity between the two events (at least 30 kyr), which is consistent with the petrological reconstruction of the PCD derivation from a *post-UP* system evolved from the UP magma residue (Braschi et al., 2012).

The UP rhyolites show a homogeneous composition, with chemical and isotopic characteristics well distinct from those of the PCD rhyodacites (Braschi et al., 2012, 2022; Fig. S1 in the Supplement). PCD lavas instead display compositional variations, depicting well-defined time-dependent trends towards less evolved compositions (Fig. S1). The mafic melt intruding into the UP evolved chamber generated crystal-rich clasts (CRCs) that are highly heterogeneous in composition, ranging from mainly andesite to dacite, and generally more evolved than the PCD enclaves, which instead range from basaltic andesite to andesites (Fig. S1). These enclaves display rather homogeneous geochemical and isotopic characteristics that are again well distinct from those of the CRCs hosted in the UP (Fig. S1).

Finally, petrographic, geochemical, and isotopic evidence (Braschi et al., 2012, 2022) has indicated a notable increase in the extent of the mingling process with time (i.e., from the UP to the PCD stage and from the oldest to the youngest domes). This argues for a change in the conditions of magma interaction (e.g., compositional contrast and time of interaction) between the two phases of activity, as further discussed in Sect. 5.

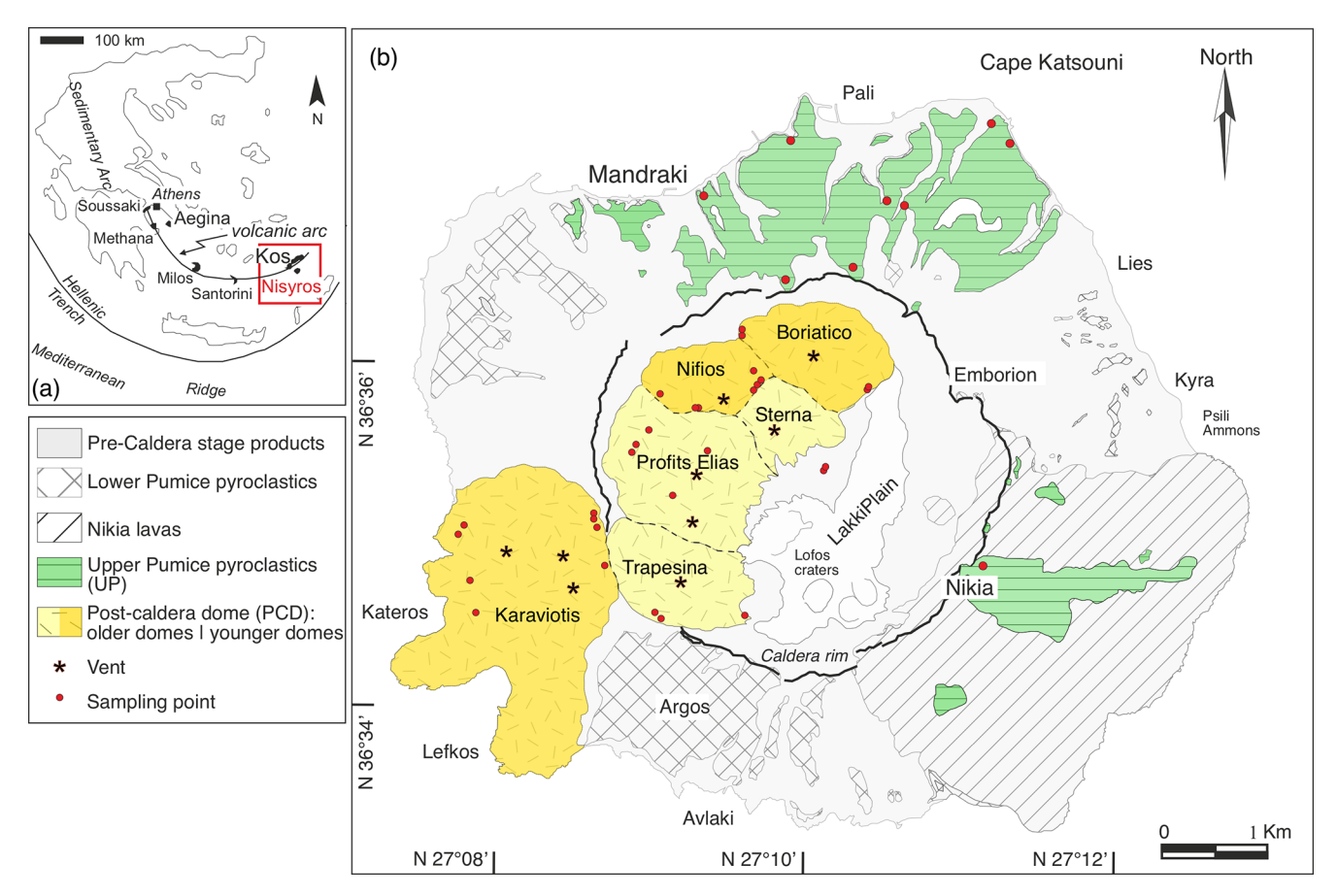


Figure 1. Geological sketched map reporting the distribution of pyroclastic deposits and lava domes erupted in the recent activity of Nisyros. In green – the Upper Pumice (UP) pyroclastites, in yellow – the six main dome edifices of the Post Caldera Domes (PCD). Different shades of yellow refer to the relative age of the domes according to Vougioukalakis (1993) and Dietrich (2018).

3 Samples and methods

For the purpose of this study, selected representative samples were chosen for mineral chemistry analysis for a total of 11 samples from UP and 17 from PCD (Table S1 in the Supplement). All data of the UP samples are available at https://ecl.earthchem.org/view.php?id=2230 (last access: 1 October 2025) and in Mastroianni et al. (2022). The plagioclase composition of the PCD samples is reported in the supplementary material 2 of Braschi et al. (2014). New, unpublished data on olivine, pyroxenes, amphibole, oxides, and glasses of the PCD and CRC samples reported in this study are provided in Table S2.

Mineral chemistry analyses were performed at the microprobe joined laboratory of the CNR-IGG and the Department of Earth Sciences of Florence. The instruments used were the JEOL Superprobe JXA8600 and the new JXA8230, equipped with four and five wavelength dispersion spectrometers, respectively. Analytical conditions were a 15 kV accelerating voltage, 10 to 20 nA beam current, and focused beam, except for feldspar and glasses, where the beam was defocused to 5

and 10 µm, respectively, to reduce diffusion effects on alkali. See the Supplement and Table S2g for further details.

4 Petrography and mineral chemistry

The petrography (Figs. 3 and 4, S2 and S3) and mineral assemblage composition (Figs. 5–7) of both PCD and UP juveniles are described hereafter. We distinguish phenocrysts ($>0.6\,\mathrm{mm}$), micro-phenocrysts (0.4– $0.6\,\mathrm{mm}$), microlites (0.1– $0.2\,\mathrm{mm}$), and groundmass ($<0.1\,\mathrm{mm}$) according to their crystal size.

4.1 Petrography of the UP pumice and PCD lavas

The rhyolitic UP pumice samples are low porphyritic (< 5 vol % of phenocrysts) and show a glassy, highly vesiculated, fluidal groundmass (Fig. 3c, d). In contrast, the PCD rhyodacites are highly porphyritic (up to 30 vol %–40 vol % of phenocrysts) with a cryptocrystalline to glassy groundmass (Fig. 3g).

Plagioclase is always the most abundant phenocryst both in UP pumice and PCD lavas. It is also present as micro-

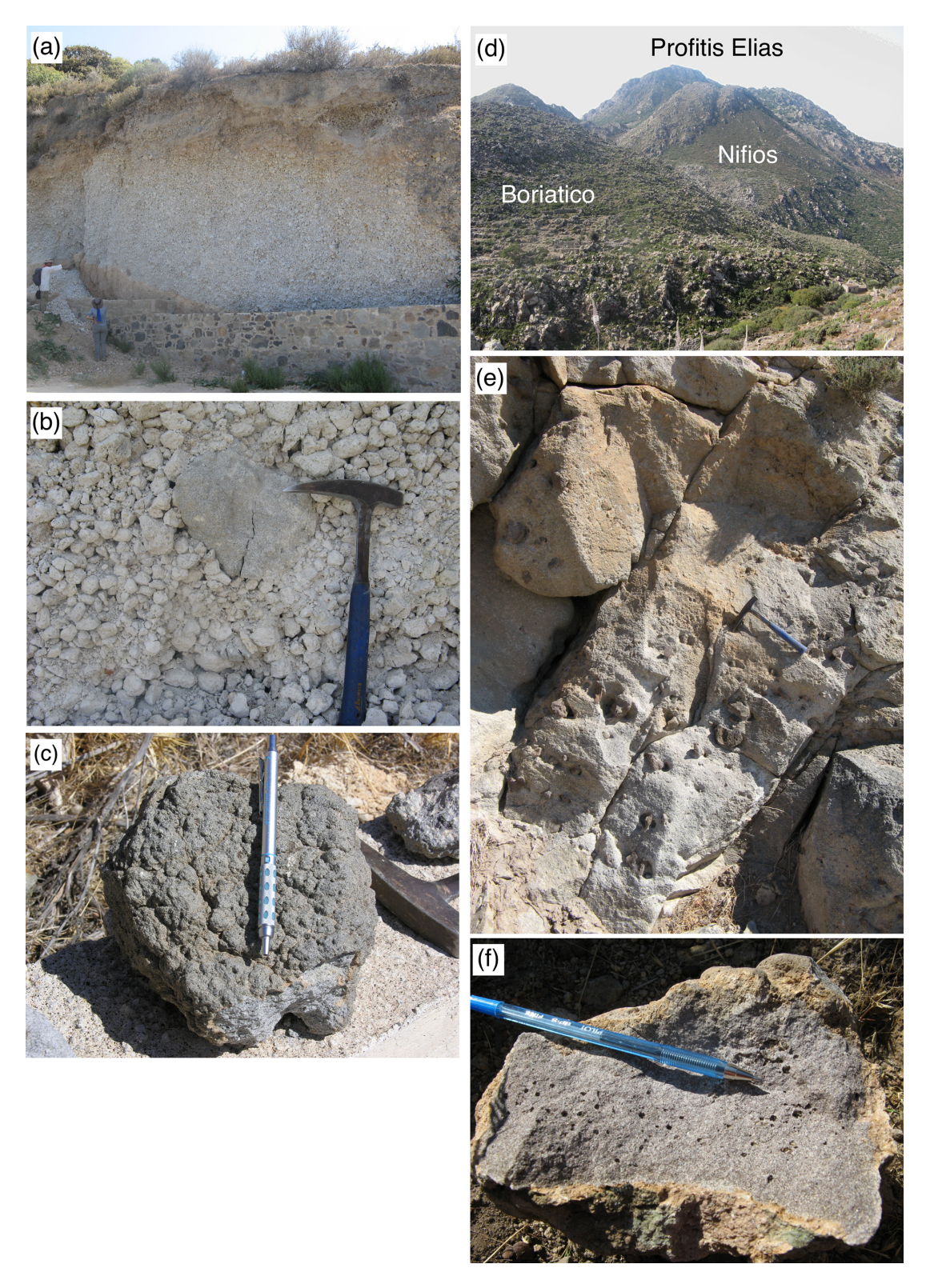


Figure 2. Field images of representative outcrops for UP (a-b) and PCD (d-e). (a) Basal fallout deposit near the village of Mandraki; (b) detail of the pumice fallout deposit hosting a representative example of Type-A CRC; (c) representative sample of Type-C CRC with a crenulated surface; (e) field overview of Boriatico, in the foreground, and Nifios domes, with the two peaks of the Profitis Elias dome in the background; (f) outcrop of the Trapesina lava dome hosting enclaves of variable sizes; (g) representative sample of a magmatic enclave found in the Boriatico lava dome, characterized by typical rounded vesicles and a chilled margin.

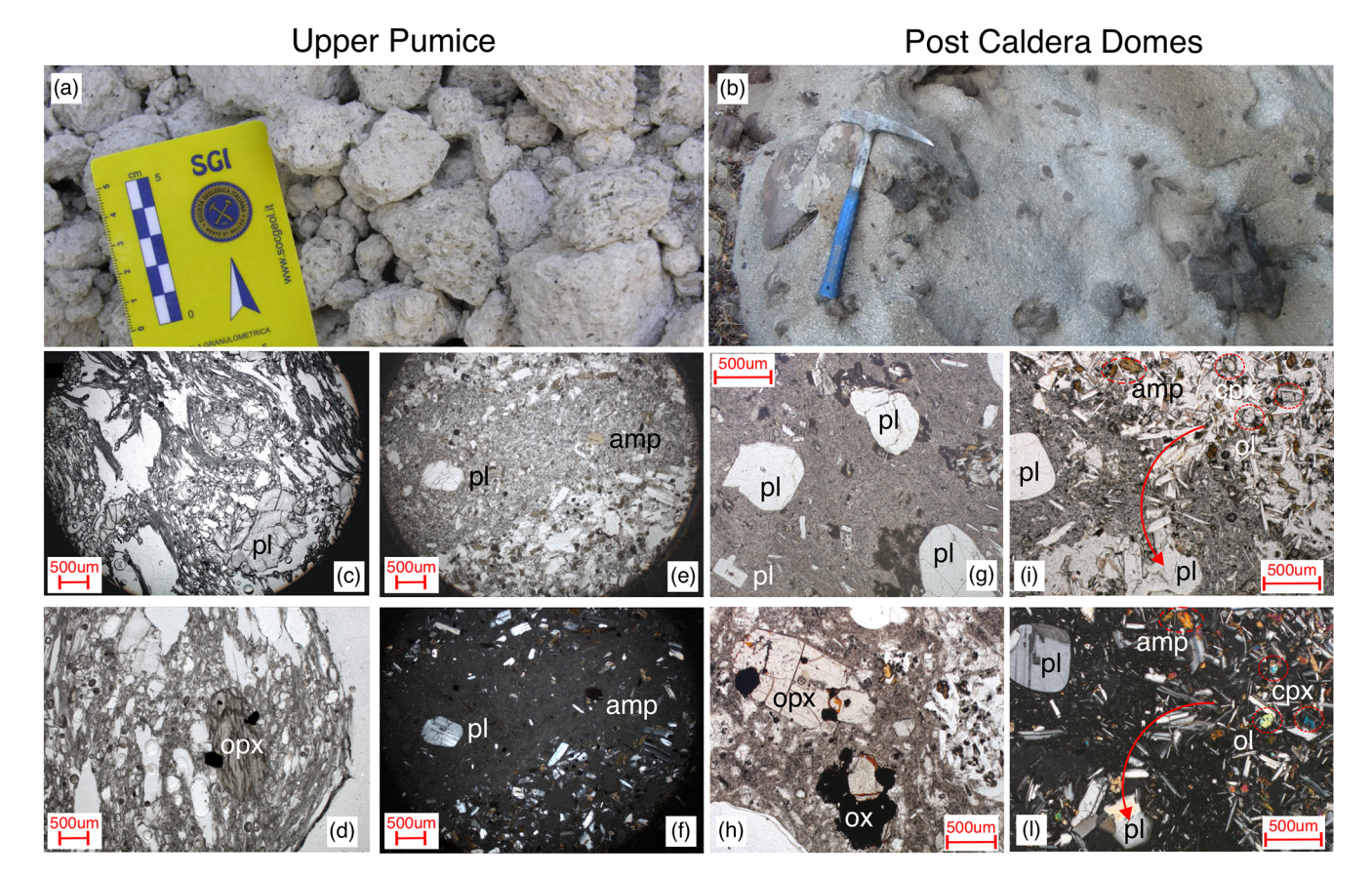


Figure 3. Hand specimen (**a–b**) and microscope (**c–l**) images showing and comparing the main petrographic features characterizing UP pumice samples and PCD lavas. (**a**) Detail of the fallout deposit composed of white pumice lapilli; (**b**) detail of the Karaviotis dome outcrop where abundant enclaves are exposed on the surface; (**c–d**) representative plane-polarized microscope images of UP pumice with a fluidal, highly vesicular structure and plagioclase (**pl**) and orthopyroxene (opx) phenocrysts, aggregated with oxides (ox); (**e–f**) contact between pumice and CRC in a banded pumice sample (plane- and cross-polarized light, respectively); (**g–h**) representative plane-polarized microscope images of PCD lava with a glassy, cryptocrystalline groundmass and phenocrysts of subhedral, clear plagioclase and orthopyroxene (aggregated with oxides); and (**i–l**) contact between the lavas and enclave with incipient disaggregation (plane- and cross-polarized light, respectively). cpx – clinopyroxene, ol – olivine, amp – amphibole.

phenocryst and microlite, and it is the prevalent mineral phase forming the PCD lava groundmass. Phenocrysts and micro-phenocrysts in UP pumice have a euhedral shape and are characterized by concentric or oscillatory zoning, they are frequently broken, and they are found as single crystals or aggregated (Fig. 3c). In the PCD lavas, plagioclase instead shows wide variability and can be subdivided into different types (Braschi et al., 2014). The most representative type includes large (up to 5 mm), poorly zoned phenocrysts and micro-phenocrysts, with a subhedral, rounded shape (Fig. 3g). The other types consist of (i) subhedral phenocrysts and micro-phenocrysts with inner dusty sieved zones and a thin, clear rim; (ii) euhedral phenocrysts and micro-phenocrysts with coarsely sieved cores; and (iii) euhedral unzoned micro-phenocrysts and microlites.

Orthopyroxene is subordinate to plagioclase in both lithologies and mainly occurs as subhedral phenocrysts and micro-phenocrysts, usually found in aggregates with oxides (Fig. 3d, h). Clinopyroxene is rare in UP pumice and is generally present as micro-phenocrysts and microlites. In PCD lavas, clinopyroxene is less abundant than orthopyroxene as phenocryst and micro-phenocryst, but it becomes prevalent as microlites and groundmass. Clinopyroxene phenocrysts often occur as aggregates with orthopyroxene and oxides with a subhedral shape (Fig. S2c).

Olivine is rare and small ($< 300\,\mu m$) in the PCD lavas, usually with an anhedral, rounded shape and an oxidated rim (Fig. S2a).

A key feature that differentiates PCD lavas from UP pumice is the presence of several aggregates in the former, revealing the multi-component nature of this magma: (1) glomerocrysts (0.6–5 mm) of resorbed quartz, frequently aggregated with subhedral plagioclase and occasionally with clinopyroxene; (2) mafic aggregates (0.6–2 mm), formed by phenocrysts and micro-phenocrysts of orthopyroxene and oxides, clinopyroxene and oxides, or olivine with ortho- and

clinopyroxene plus oxides; and (3) micro-enclaves (0.5 to 4–5 mm) with a rounded shape and microcrystalline to acicular textures (Fig. S2e), representing small fragments of the main mafic enclaves dispersed inside the rhyodacitic dome lavas. The micro-enclaves are more abundant in the younger dome (i.e., Boriatico; see Fig. 1), indicating the increasing extent of mechanical disaggregation (magma mingling) with time within the PCD system. These features are absent in the UP, where micro-mingling is less developed than in the PCD (Braschi et al., 2014, 2022).

4.2 Petrography of the UP CRCs and PCD enclaves

At the macroscale, both CRCs and PCD enclaves show sharp contacts with their host (Fig. 2b, e) and appear as discrete bodies within their pumice or lava hosts. In the UP, interbedded contacts between the pumice and CRCs are also frequently observed (Fig. S3a, b). In the PCD, the contacts between enclaves and host lavas are frequently characterized by a chilled margin with variable thickness (Fig. S3c, g). They usually show crenulate or convolute surfaces (Fig. 4a–c).

At the microscale, the boundaries between the PCD enclave and the host lavas show evident disaggregation features (Fig. 3i, 1) or evidence of single-crystal exchange (Fig. S3d, g). This corroborates the origin of the enclaves as discrete bodies when both the refilling and the host magmas were still molten (Braschi et al., 2012, 2022).

The CRCs show heterogeneous textures (Mastroianni et al., 2022) with a paragenesis dominated by plagioclase with subordinate ortho- and clinopyroxene or amphiboles, in variable proportions, and minor oxides.

CRCs have previously been classified into three different types (Braschi et al., 2022; Mastroianni et al., 2022) according to textures. Type-A CRCs have a highly vesiculated, open microcrystalline structure (Fig. 4a, d, e); Type-C CRCs have a well-defined network of elongated, joined microcrystals forming a diktytaxitic structure (Fig. 4b, f, g); and Type-B CRCs have intermediate characteristics between Type-A and Type-B.

In all types the groundmass is formed by a microlite network of plagioclase and amphiboles in variable proportions. Phenocrysts and micro-phenocrysts are rare, especially in Type-A, where the size distribution is more continuous.

Amphibole is present in all CRCs, but it occurs in different proportions (more abundant in Type-C) and shapes. In Type-C, amphiboles show a tabular to elongated shape ranging in size from micro-phenocrysts to microlites and form a network with acicular plagioclase (Fig. 4f, g). In the other two types (A and B), they are usually tabular with euhedral shapes, similar to plagioclase (Fig. 4d, e). In some cases, amphibole replaces clinopyroxene or forms symplectitic intergrowth aggregates with it, which are interstitial in the plagioclase network (Fig. S4a). Clinopyroxenes are present as subhedral crystals with evident zoning or form aggregates with orthopyroxene (Fig. S4b, e). Olivine occurs as rare micro-

phenocrysts and microlites, showing subhedral shapes with partially oxidized rims (Fig. S4b). Oxides are sporadic, usually appearing as micro-phenocrysts with subhedral shapes.

The PCD enclaves have hypo-crystalline, diktytaxitic textures, with a low porphyritic index (< 5 vol %) and a paragenesis dominated by acicular plagioclase and amphibole (Fig. 4c, h, i), with minor clinopyroxene and oxides and subordinated olivine. Phenocrysts mainly consist of dusty sieved plagioclase with a subhedral shape (resembling those present in the lava host, Fig. S3h) or minor euhedral plagioclase with a tabular shape and resorbed cores. Amphiboles are occasionally zoned with an elongated to acicular shape, and they form, together with plagioclase, the diktytaxitic network typical of quenched magma batches (Fig. S4f). Clinopyroxene is usually small and present as isolated micro-phenocrysts or microlites (Figs. S2f and S4c), frequently showing amphibole overgrowth; occasionally it also occurs as olivine rims (Fig. S4d). Olivine is present only in a few enclaves (irrespective of their evolutionary degree), occurring mainly as micro-phenocrysts, usually with a subhedral, rounded shape and oxidized rims (Figs. S2b and S4d). Oxides are small with a euhedral shape and variable abundance among the enclave population.

Similar to the PCD lavas, the enclaves host different types of aggregates: (1) mafic aggregates, similar to those found in the dome lavas; (2) gabbroid aggregates with olivine, plagioclase, pyroxenes, and oxides; and (3) sub-enclaves, with a structure and mineral assemblage similar to those of the main enclaves in which they are enclosed but with a smaller grain-size groundmass and a totally aphyric texture.

According to their petrological characteristics, the CRCs and PCD enclaves are both interpreted as magmatic enclaves formed by the mechanical interaction between a mafic refilling magma and an evolved host. Further, their microcrystalline diktytaxitic network made of acicular crystals forming the groundmass and the occurrence of chilled margins indicate that they formed by rapid crystallization due to the undercooling generated by a high thermal contrast (e.g., Blake and Fink, 2000; Coombs et al., 2002). For the former, we maintain the CRC term used in Braschi et al. (2022) both for consistency and to stress the importance of their volcanological origin, which is different from that of the PCD enclaves.

4.3 Mineral chemistry

The mineral chemistry of the investigated volcanic products has been determined in selected, representative samples (Table S1). Results are described below and reported in Table S2a-f.

4.3.1 Olivine

In the UP, only a few olivine analyses have been performed on micro-phenocrysts from the pumice and two CRC samples (Type-A and Type-C). In the pumice, two cores have a

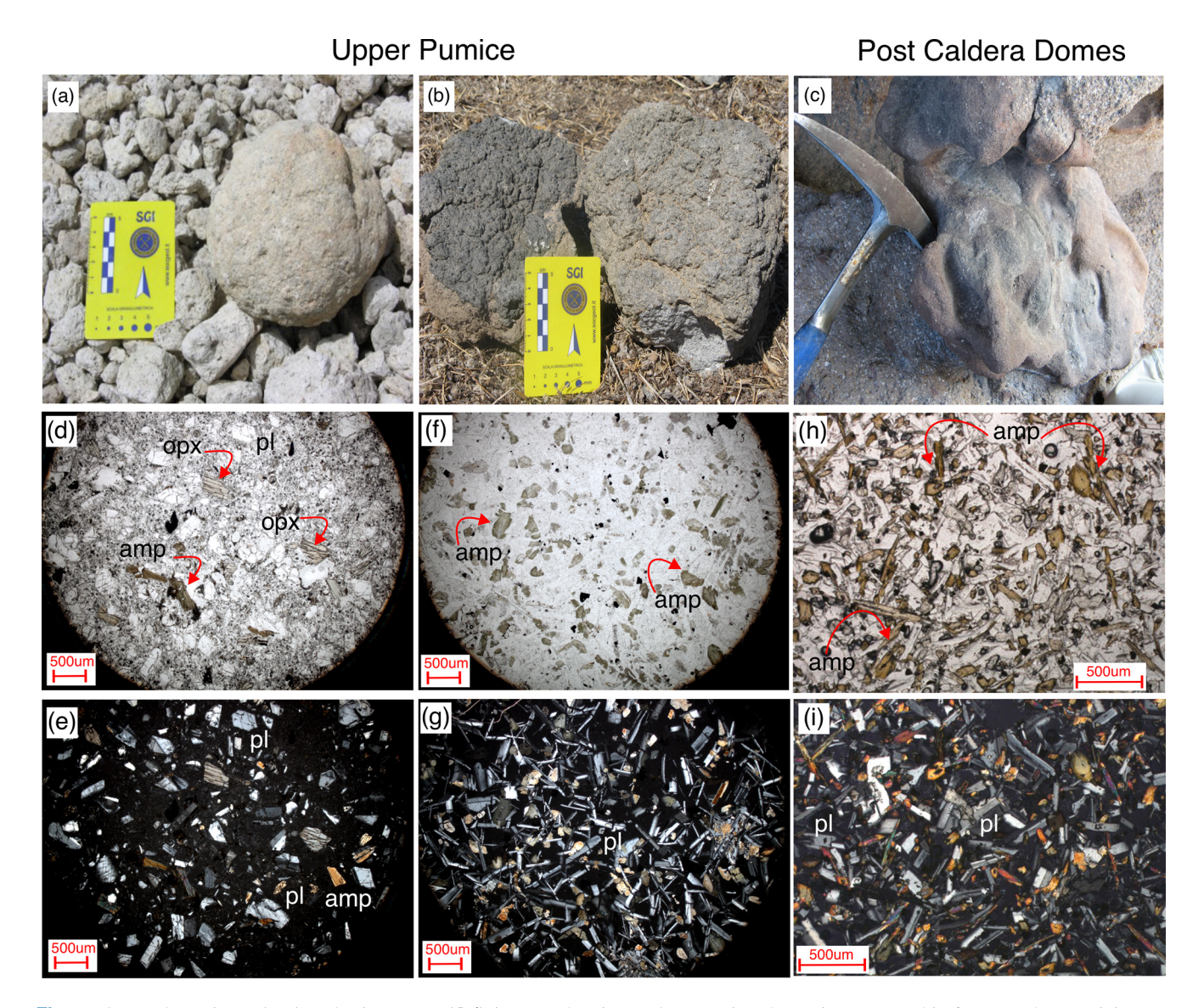


Figure 4. Hand specimen (a-c) and microscope (d-i) images showing and comparing the main petrographic features characterizing UP CRCs and PCD enclaves. (a-b) Hand specimen of a UP CRC Type-A and Type-C sample collected in the fallout and lag-breccia deposit, respectively; (c) representative image of a magmatic enclave in the PCD with a typical fluidal shape; (d-e) plane- and cross-polarized light microphotograph of a CRC Type-A sample, showing a typical open structure with broken crystals of mainly plagioclase (pl), amphibole (amp), and orthopyroxene (opx); (f-g) plane- and cross-polarized light microphotograph of a CRC Type-C sample, showing the typical diktytaxitic structure of the groundmass with interconnected acicular plagioclase (pl) and tabular amphibole (amp); and (h-i) plane- and cross-polarized light microphotograph of a PCD enclave, showing the typical diktytaxitic structure of the groundmass characterized by a network of elongated plagioclase (pl) and amphibole (amp).

low forsteritic composition at Fo_{68} and one core at Fo_{81} . In CRCs, the analyzed olivine is normally zoned with cores at Fo_{78-83} and rims between Fo_{77-79} (Fig. 5). In PCD, olivine has been analyzed in both lavas and enclaves, showing similar compositions with homogeneous cores at Fo_{84-86} in phenocrysts and micro-phenocrysts. Phenocrysts show negligible zoning, whereas micro-phenocrysts display a relatively small normal zoning down to Fo_{77} rims. Microlites mainly have Fo_{82-84} composition without evident zoning. In general,

no relevant compositional variations are observed from the older to the younger PCD systems (Table S2a).

4.3.2 Orthopyroxene

Orthopyroxenes are enstatite with a large range of Mg# from 0.54 to 0.82 (Table S2b).

In UP pumice and PCD lavas, orthopyroxene displays similar compositions overlapping at Mg# between 0.58–0.60 (Figs. 6a, S5a, b). This is also confirmed by the compara-

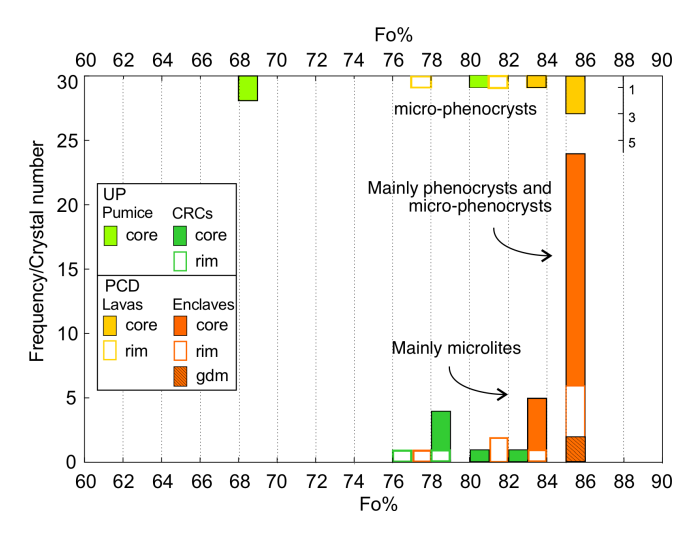


Figure 5. Histogram of core—rim olivine compositions, expressed as Fo % (forsterite) content, in the UP and PCD juveniles. Colors distinguish the UP pumice (light green) and CRCs (green) from the PCD lavas (yellow) and enclaves (orange). Filled, open, and banded histograms represent the core, rim, and groundmass (gdm), respectively, as shown in the legend.

ble content of minor elements such as Al₂O₃, MnO, TiO₂, and CaO (Fig. S6a, b; Table S2b). In detail, a small shift towards a more Mg-rich composition can be recognized in the orthopyroxenes from the PCD lavas with respect to pumice, with Mg# up to 0.67 (Figs. 6a, S5a, b). Small inverse zoning is observed in both the orthopyroxene from the pumice (e.g., from 0.59 to 0.60 Mg#) and the lavas (e.g., from 0.60 to 0.61 Mg#). Microlites are only present in the PCD lavas showing higher Mg# (0.75–0.78), CaO, and Al₂O₃ and lower MnO than phenocrysts and micro-phenocrysts (Fig. S6a, b).

In CRCs and enclaves the orthopyroxene composition is more variable and scattered, especially in the CRC samples (Fig. 6b).

In the PCD enclaves, phenocrysts and micro-phenocrysts show a narrow peak at Mg# 0.61 (both cores and rims), which overlaps with that of the phenocrysts and micro-phenocrysts in the lavas, with only minor scatter toward Mg-rich compositions. Notably, the groundmass shows a distinct, less evolved composition (Mg# 0.73–0.80), again overlapping with that of the groundmass of the corresponding lavas.

In the CRCs, orthopyroxene shows a larger compositional variability. It occurs mainly as microlites, grouped around three well-distinct Mg# intervals at 0.52–0.55, 0.62–0.66, and 0.79–0.81. The largest variability was found in Type-A samples, including normally zoned micro-phenocrysts with a high-Mg# core (0.77–0.81) and rims down to Mg# 0.56–0.58. (Fig. S5a).

The distinctive behavior of orthopyroxenes belonging to the CRCs with respect to those found in pumice, lavas, and enclaves is also confirmed by Al₂O₃, CaO, TiO₂, and MnO (Fig. 6a, b; Table S2b). In particular, CRC orthopyroxene defines a broad inverse correlation between Mg# and Mn, with an absolute lower MnO content than that of all the other lithotypes (Fig. S6b). This indicates that the orthopyroxenes in the CRCs formed within a different magmatic environment following specific crystallization paths. The increase in MnO follows that in FeO, as expected in an evolving magma. Notably, the observed trend is defined by microlites, which provide snapshots of the crystallization history of the magma batch. Their progressive compositional variation testifies to the rapid liquid evolution during cooling of the CRC magma when intruding into the pumice host. Accordingly, significant chemical variation among microlites is used in the following sections as evidence of rapid crystallization.

4.3.3 Clinopyroxene

Clinopyroxenes have a general augitic–diopsidic composition, with large Mg# variation, ranging from 0.65 to 0.85 (Table S2c).

Only two micro-phenocrysts were analyzed in the UP pumice, with Mg# of 0.68 and 0.72. In contrast, a few microphenocrysts and many microlites were investigated in the PCD lavas, depicting a wide variability in core composition, with a mode from Mg# 0.78 to 0.85 (Fig. 6c). However, a few cores display lower Mg# between 0.75 and 0.72. Rims and groundmass encompass the same Mg# range as the cores. Zoning is limited and, when present, always reversed (Figs. 6c, S6c).

In CRCs, clinopyroxene crystals are mainly microphenocrysts, depicting a well-defined peak at high Mg# (0.84–0.85), but a group of crystals at lower Mg# (0.68–0.76) is also present. This second group also includes the rims of the high-Mg# micro-phenocrysts, hence having large normal zoning (Figs. 6d, S5c).

The clinopyroxene of the PCD enclaves shows a marked variability, broadly overlapping with the composition of the crystals of the dome lavas (Fig. 6d), with most crystals in the Mg# range of 0.79–0.85. Zoning is mainly normal for microphenocrysts (Figs. 6d, S5c), whilst it is absent for microlites. Within the PCD system, no systematic variations in clinopyroxene composition with age are observed.

Differently from orthopyroxene, clinopyroxene show the same zoning pattern in CRCs and PCD enclaves.

In general, Mg# is not correlated with CaO, in contrast to Na₂O and MnO, which show an inverse correlation, with CRCs showing on average lower MnO than all the other lithotypes, similar to orthopyroxene (Fig. S6d). Al₂O₃ (and TiO₂) shows a complex distribution compared to Mg# (Fig. S6c): some crystals define a trend of decreasing Al (and Ti) with Mg# (pattern 1 in Fig. S6c), whilst others show the opposite (pattern 2 in Fig. S6c). High-Mg# phenocryst cores belong only to pattern 1, whilst groundmass and most of the microlites and rims follow pattern 2 (Fig. S6c).

The increase in the Al content with decreasing Mg# suggests that clinopyroxene crystallizes when plagioclase is not

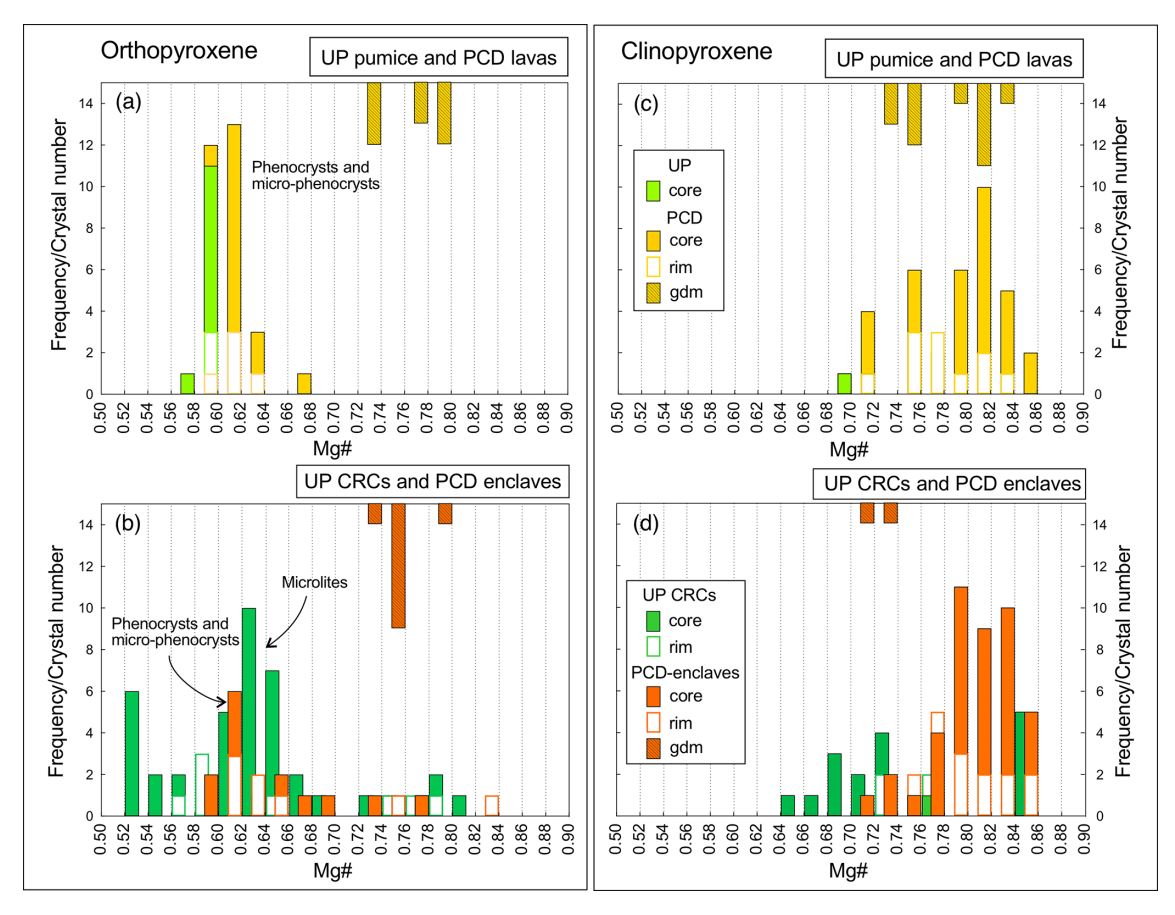


Figure 6. Histogram of core–rim pyroxene composition in the UP and PCD juveniles. (**a–b**) Orthopyroxene composition, expressed by Mg#, calculated as molar $Mg/(Mg-Fe^{2+}+Fe^{3+}+Mn)$, comparing pumice with PCD lavas (**a**) and CRCs with PCD enclaves (**b**). (**c–d**) Clinopyroxene composition, expressed by Mg#, calculated as molar $Mg/(Mg-Fe^{2+}+Fe^{3+}+Mn)$, comparing pumice with PCD lavas (**c**) and CRCs with PCD enclaves (**d**). Symbols and colors are the same as those in Fig. 5 and are shown in the legend (dark green color refers to CRCs).

stable, likely reflecting different crystallization pathways occurring under different conditions (in temperature or water content) with respect to pattern 1.

4.3.4 Plagioclase

Plagioclase display a very large compositional variability from anorthite to andesine and oligoclase, indicating wide zonings and complex crystallization histories.

The history of PCD plagioclases and, partially, those of the UP, were widely discussed in Braschi et al. (2014). For this study, we compare the existing data with the new data acquired on the plagioclases from the UP CRCs to explore possible differences or analogies.

An evident peak at low An% content (An_{25-35}) is observed for plagioclase belonging to PCD lavas, enclaves, and UP pumice (Fig. 7a–c) and corresponds to groundmass crystals and large, subhedral phenocrysts (Figs. 3g, S3g, h). This agrees with the rhyodacitic composition of the melts forming the PCD lavas and UP pumice but contrasts with the less

evolved signature of PCD enclaves. In any case, these low-An phenocrysts usually show small, normal zoning in the UP pumice, while in the PCD lavas, zoning is more variable and includes crystals with reverse zoning, with rims at intermediate composition (up to An_{60-70}). In the PCD enclaves, low-An phenocrysts show dusty sieved bands (Fig. S2h) and large inverse zoning recorded by clear, thin rims at An_{70-80} up to An_{90} (Fig. 7a–c). Notably, low-An phenocrysts are not found in the CRCs.

High-An plagioclases are not found in the UP pumice but are recurrent in the PCD lavas, where two peaks are defined at An_{65-70} and An_{75-80} by some phenocrysts, microphenocrysts, and minor microlites with a euhedral shape (Figs. 7b, S3h, g). In the PCD enclaves, the majority of the plagioclase population is characterized by high-An composition, as expected for basaltic andesite. They do not show uniform compositions but define two distinct peaks: euhedral phenocryst cores cluster at An_{85-95} (Fig. 7c), whereas groundmass, microlites of the diktytaxitic network, and micro-phenocrysts cluster at An_{70-75} .

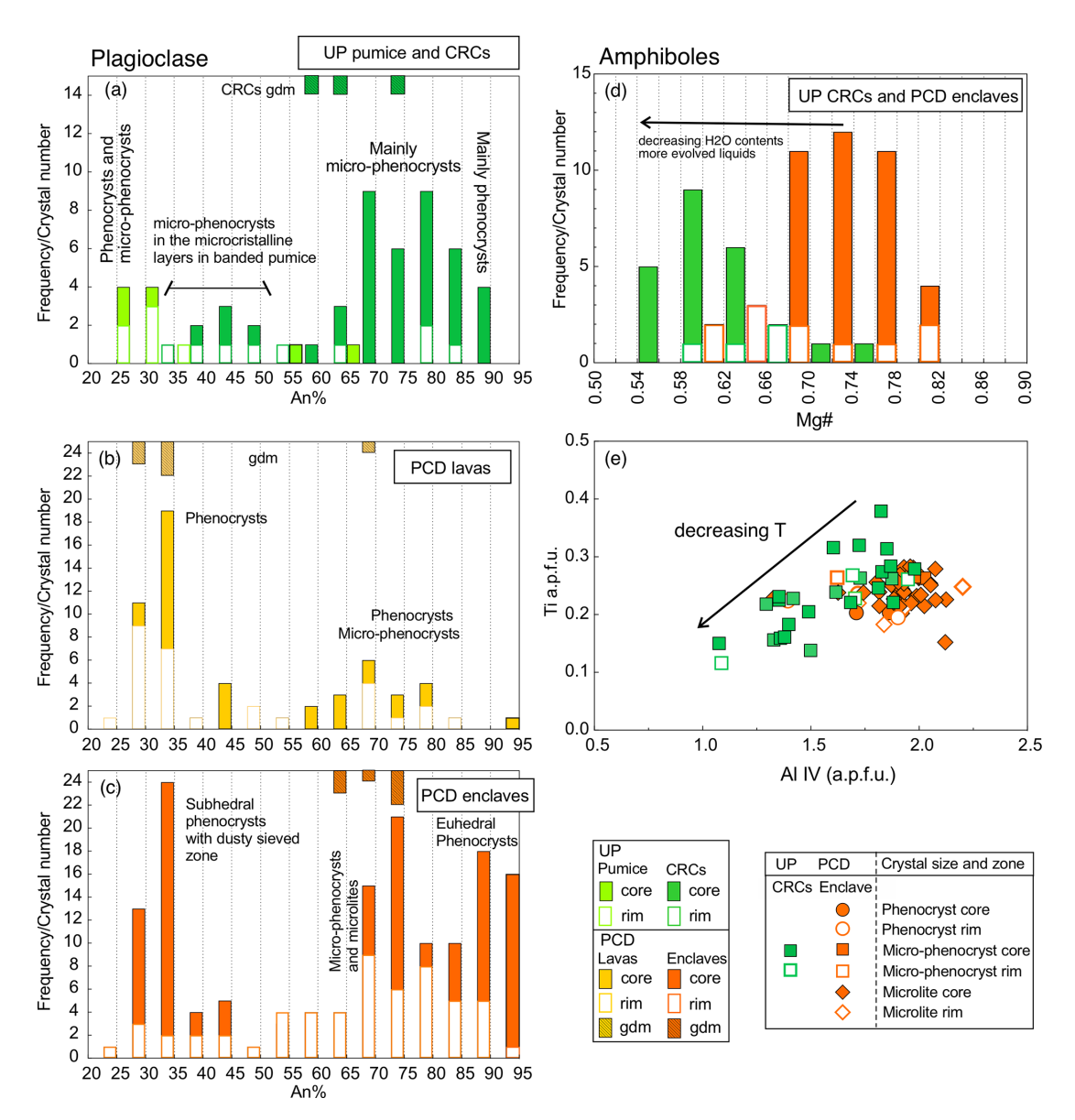


Figure 7. Principal compositional characteristics of plagioclase (a–c) and amphiboles (d, e) analyzed in the UP and PCD products. (a–c) Histograms of core–rim plagioclase composition in the UP (a), PCD lavas (b), and enclaves (c); (d) histogram of core–rim amphibole composition in the UP CRCs and PCD enclaves; and (e) correlation plot of Ti versus Al^{IV}, expressed as atoms per formula unit (a.p.f.u.), which is indicative of temperature variation. Colors are the same as in Fig. 6, and symbols refer to different crystal sizes (phenocrysts, micro-phenocrysts, and microlites) and zones (core and rim), as shown in the legend.

The plagioclase from CRCs broadly overlaps with the compositional range of that of the PCD enclaves at An_{65-85} . It occurs mostly as micro-phenocrysts, with only a few (normally zoned) phenocryst cores at An_{85-90} . A few intermediate compositions at An_{40-45} were found only in phenocrysts and micro-phenocrysts analyzed in a microcrystalline layer of a banded pumice, suggesting the presence of an intermediate, hybrid boundary between the UP host and the CRC-forming magma.

4.3.5 Amphiboles

Amphiboles are the dominant mineral phase of most PCD enclaves and Type-C CRCs, forming the diktytaxitic network together with plagioclase. They are less abundant in Type-A and Type-B CRCs, where plagioclase and orthopyroxene predominate. In the UP pumice and PCD lavas, amphiboles do not crystallize and are occasionally present only as accidental crystals entrained form the mafic magma.

The amphibole composition is shown in Figs. 7b–c and S7 and is reported in Table S2d. Amphiboles are classified

as ferri-titan tschermakite with minor magnesio-hornblende found in the CRCs (Fig. S7b) according to Ridolfi (2021) and Locock (2014). In general, they partially overlap in composition yet show well-distinct trends between the two populations characterizing the CRCs and PCD enclaves.

The Mg# of amphibole in CRCs ranges from 0.55 to 0.75, with a mode value around 0.61 at a less evolved composition than that in PCD enclaves, which shows a wide variation with a main cluster between 0.68 and 0.78 (Fig. 7d). Zoning is reversed (but limited) in CRC amphibole, whilst it is mainly normal in PCD enclaves.

Other compositional parameters confirm the distinct behavior of the amphiboles from PCD enclaves and CRCs (Fig. S7a). Al₂O₃ wt % in the enclaves is clustered at 12 wt %–13 wt %, with values up to 15 wt %; in CRCs it is instead more heterogeneous, ranging from 6 wt % to 13 wt %. The distribution of Al in the amphibole is a parameter that depends on the different physico-chemical conditions of crystallization, and its variability can be correlated to (i) magma evolution (affecting the Si-Al^{IV} substitution), (ii) temperature (driving the AlVI-Ti substitution), (iii) oxygen fugacity (Al^{VI}-Fe³⁺ substitution), and (iv) pressure. In Fig. 7e the amphiboles from CRCs show a broad correlation between AlIV and Ti, indicating a decrease in temperature that is consistent with progressive magma cooling during amphibole crystallization (Krawczynski et al., 2012; Ridolfi, 2021). In contrast, amphiboles in the PCD enclaves do not show systematic variations. This indicates that the mafic magmas forming the enclaves had a similar temperature and that cooling was efficient and rapid enough to produce massive crystallization, buffering the amphibole composition.

Al^{VI} is lower and less variable in CRC amphiboles than in PCD enclave amphiboles, where it is also broadly correlated with Mg# (Fig. S7d). These variations in Al^{VI} are probably linked to the effect of oxygen fugacity, which is also reflected by $Fe^{3+}/(Fe^{3+}+Fe^{2+})$ behavior (Fig. S7c). In particular, among the PCD enclaves, those erupted in the older domes show a higher Fe^{3+} content, indicating a possible decrease in fO_2 over time. Overall, the amphibole data indicate higher fO_2 , faster cooling, and a less evolved composition for PCD enclaves than CRCs.

4.3.6 Oxides

Only a few oxides were analyzed (Table S2e). They are Fe–Ti oxides, most of which belong to the ulvöspinel–magnetite series, with 20 % ulvöspinel content, whereas the others belong to the ilmenite–hematite series, with 79 % ilmenite content, following the scheme of Stormer (1983). The latter occur mainly in the PCD lavas as phenocryst or micro-phenocryst aggregates with pyroxenes. A few ilmenites are present in the UP (pumice and CRCs) and in the enclaves of the old PCD, but none was found in the younger PCD enclaves, where only magnetite microlites are present. In general, Fe–Ti oxides are pristine, unzoned, and compositionally homogeneous irre-

spective of crystal size. Only a small variability in their composition is detectable in the younger PCD enclaves, which shows a slight decrease in the ulvöspinel component towards the younger PCD enclaves.

4.4 Glass chemistry

The matrix glass composition of UP and PCD products is reported in Mastroianni et al. (2022) and in Table S2f and shown in Fig. S8.

All glasses have a highly evolved composition, with silica content over 74 wt % and K_2O ranging from 3.5 wt % to 6 wt %, showing a general overlap among all lithotypes, although those from the PCD depict a large scatter.

In the UP, pumice glasses are more homogeneous than glasses from the CRCs (similar to whole-rock compositions), with an average content of 77.5 wt % and small variation for all the other major elements. The CRC glasses, although less homogeneous, depict systematic behavior, outlining well-defined compositional ranges depending on samples and texture types.

For the PCD, only a few consistent glass analyses could be obtained from dome lavas due to the cryptocrystalline texture of the groundmass, especially in the younger domes. Most analyses belong to the older PCD and show predominantly silica values > 78 wt % and K₂O up to 5.05 wt %, being slightly more evolved than the glasses of the UP pumice (Fig. S8a). Glasses from the younger PCD have slightly lower silica content compared to the older ones and more variable content in the other major elements (Fig. S8 and Table S2f). On the other side, the glasses from PCD enclaves are generally less evolved than those of PCD lavas, with silica content ranging from 74.8 wt % to 78.6 wt %, thus encompassing the whole silica range. They also show a larger compositional scatter than CRC glasses, with less systematicity related to the single sample, although Al₂O₃ and FeO show a broad inverse correlation with silica (Fig. S8b, d). Notably, the PCD enclave glasses are found as small interstitial sects around the diktytaxitic voids and are hence prone to a higher variability depending on local crystallizing paragenesis.

5 Discussion

The mineral chemistry characteristics of the UP and PCD products depict a complex picture revealing an intimate correlation between mineral composition and petrographic characteristics.

In our previous study on plagioclase, we already demonstrated that the observed compositional bimodality in the PCD is indicative of intense single-crystal exchange phenomena between the rhyolitic host and the enclave-forming mafic melts that mingled in the magma chamber before the eruption (Braschi et al., 2014). Moreover, in situ isotopes revealed that low-An plagioclase phenocrysts are inherited from the previous UP rhyolitic magma that represents the

silica-rich system from which the PCD lavas are derived through open-system evolutionary processes (*post-UP* stage of Braschi et al., 2012). PCD lavas have thus been interpreted as multi-component magmas formed by progressive mingling/mixing processes due to intrusion, dispersion, and progressive disaggregation of the mafic, enclave-forming magmas with time. With this in mind, here we evaluate the role of femic phases to further detail the dynamics of interactions and their evolution through time.

5.1 Evidence from mineral (dis)equilibrium conditions in the UP and PCD systems

During standard crystallization, each mineral phase is in equilibrium with the relative melts. Considering the large and variable compositions of the different mineral phases forming the UP and PCD products, we aim to reconstruct the crystallization conditions of the mafic phases by testing their equilibrium with the magmas from which they crystallized and thus to constrain the history and evolution of such magmas. The equilibrium conditions can be defined for each phase by the balance of its chemical components in terms of FeO-MgO exchange, relative to those of the equilibrium melt (Putirka, 2016, and references therein). To do this, the relationships between molar FeO/MgO of femic phases and equilibrium melts were compared to experimentally or thermodynamically derived Kd_{s/l} (Fig. 8). Following Putirka (2016), we used $Kd_{s/l}$ of 0.3 ± 0.03 for olivines, 0.29 ± 0.06 for orthopyroxene, and 0.27 ± 0.03 for clinopyroxene as representative of the equilibrium interval. We assumed the whole rock (Braschi et al., 2012, 2022) of the different samples to be the representative composition of melt, being aware that it may average many different components (especially for the PCD lavas). We did not use the glass composition measured in the enclaves and CRCs (Table S2g) due to its extremely evolved composition. PCD enclaves and CRCs are indeed the residual melt resulting from the final massive crystallization and are thus not representative of the magmas from which the mafic phases crystalized. Similarly, the cryptocrystalline groundmass of the PCD lavas did not allow for the analyses of consistent, representative melt composition.

Regarding olivine (Fig. 8a), all the micro-phenocrysts belonging to the PCD lavas and one from UP pumice have lower FeO/MgO_{mol} values than the equilibrium interval. They mainly fall in the Mg-enriched portion of the plot, thus being more forsterite rich than equilibrium. Notably, these olivine crystals have the same range of FeO/MgO_{mol} values as those analyzed in the respective CRCs or enclaves. This is clear evidence that they originate in the mafic melt, and they are transferred to the host rhyolitic magmas through enclave microscale disaggregation.

The olivine of the PCD enclaves, in contrast, shows FeO/MgO_{mol} values that generally overlap with the equilibrium interval, irrespective of their size, indicating that

they crystallized directly from the mafic magma and were preserved during ascent. Some of the olivine crystals show zoned rims with higher ${\rm FeO/MgO_{mol}}$ values, corresponding to a less forsteritic composition (down to ${\rm Fo_{77}}$), indicating crystallization from a magma that was progressively evolving during enclave quenching. This behavior is indeed a consequence of the rapid melt evolution during the specific process of enclave formation (Bacon, 1986; Anderson et al., 1984), where the evolving, transient melt is not preserved. The olivines hosted in the CRCs show the same shift to higher ${\rm FeO/MgO_{mol}}$, suggesting a similar process for their formation.

The interpretation of orthopyroxene distribution with respect to the calculated equilibrium $Kd_{s/l}$ (Fig. 8b) is rather complex, since crystals of different sizes or belonging to different lithologies display heterogeneous behaviors.

All phenocrysts and micro-phenocrysts analyzed in the UP pumice and PCD lavas show FeO/MgO_{mol} higher than equilibrium. Such high FeO/MgO_{mol} would be in equilibrium with a more evolved, Fe-rich host magma, with FeO/MgO_{mol} between 2.1–2.3 and 2.8, which is, in fact, consistent with that measured in some rhyolitic pumice glasses of the UP and with the calculated *post-UP* composition (Braschi et al., 2012).

We thus suggest that orthopyroxene began to crystallize in the UP magma, and its crystallization persisted during the period between the two eruptive stages (post-UP stage). During this period, the system evolved further, forming cumulates that were later incorporated by the PCD rhyodacitic melt. The abundant occurrence of this high-Fe orthopyroxene in the PCD lavas indicates the establishment of a dynamic system able to remobilize the mush cumulates likely induced by multiple intrusions of hot enclave-forming magmas (Braschi et al., 2012, 2014). Accordingly, only the groundmass orthopyroxenes of the PCD lavas result in equilibrium with the relative melts, indicating an in situ crystallization, probably during the magma ascent or shortly before eruption. Groundmass orthopyroxene can crystallize in such evolved melts because of the high SiO₂/MgO and Al₂O₃ content in the melt, together with the general reheating of the system and appropriate fO_2 conditions (i.e., Elburg et al., 2006; Larsen, 2006). Its occurrence may also imply low ascent rates and H₂O loss for the PCD lavas during their effusive emplacement, hence providing enough time to nucleate and crystallize the groundmass, in contrast to pumice.

The same FeO/MgO_{mol} shown by orthopyroxene phenocrysts hosted in the UP and PCD lavas is also observed for phenocrysts of the PCD enclaves, which, in addition, have zoned rims with compositions towards the equilibrium range. This compositional uniformity (see also Sect. 4.1 and Fig. 6a, b) is clear evidence that they formed into the same system and that their occurrence in even PCD enclaves is a consequence of the single-crystal exchange processes already observed for plagioclase (Fig. S3d and Braschi et al., 2012). The shift towards equilibrium conditions recorded by

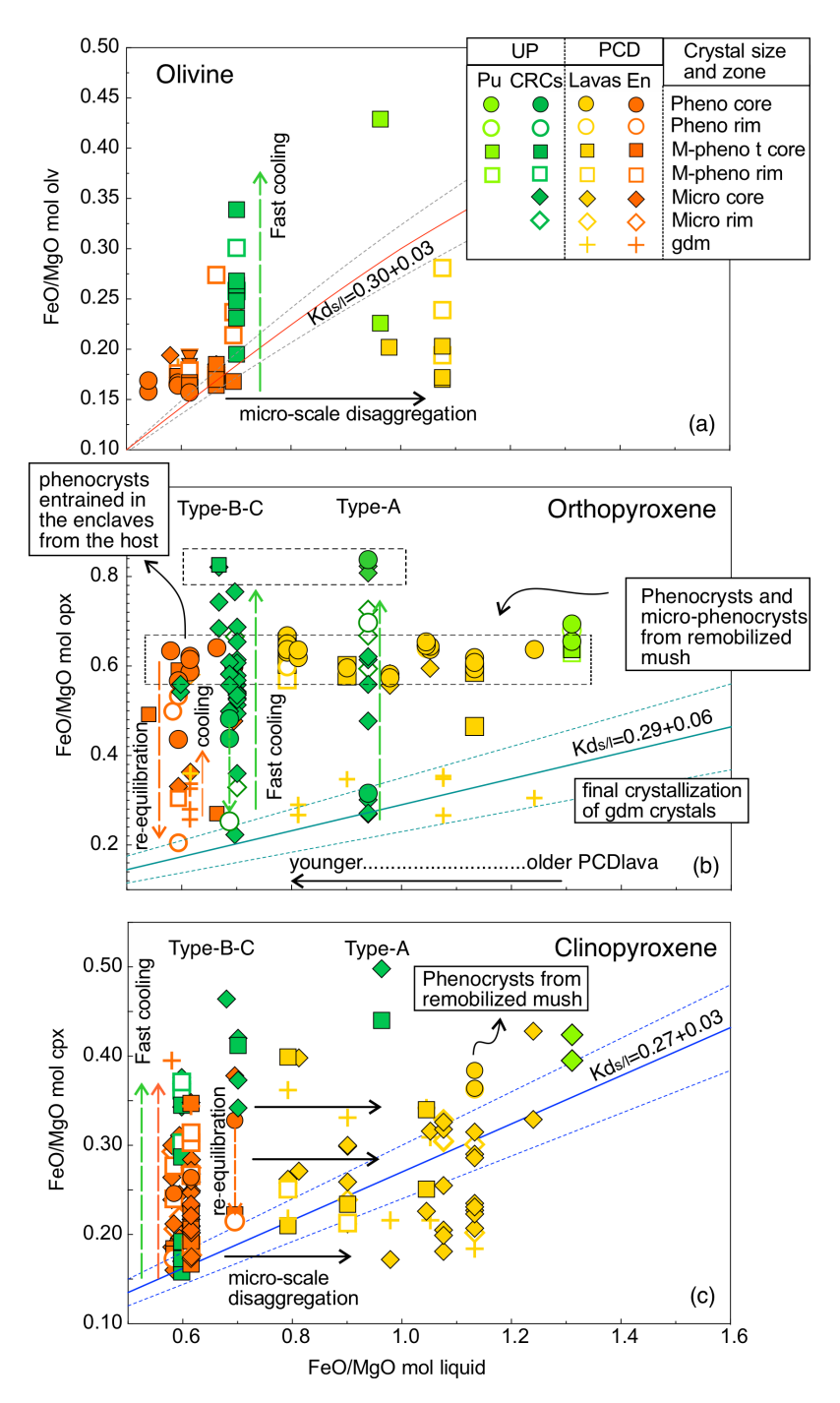


Figure 8. Plots showing the correlation between FeO/MgO_{mol} in the melt (whole rock) and FeO/MgO_{mol} in (a) olivine (ol), (b) orthopyroxene (opx), and (c) clinopyroxene (cpx) for the UP and PCD products. Melt composition is assigned to each crystal according to the respective sample: crystals analyzed in different samples will have different melt FeO/MgO_{mol} (i.e., different degrees of evolution). When whole-rock data were not available, an average representative value was calculated. Colors are the same as those in Fig. 6 and are shown in the legend together with symbols. Pu – pumice, En – enclave, En – phenocrysts, En – phenocrysts, En – phenocrystal, En Micro – microlite, En groundmass. In each plot the solid curves refer to the equilibrium values, with the relative interval of tolerance (dotted curves) as reported by Putirka (2016). Green and orange upward dashed arrows indicate compositional trends due to fast cooling in En CRCs and En PCD enclaves, respectively. Green and orange downward dashed arrows indicate the shift to re-equilibration compositions due to the entrapment of phenocrysts from the host into the En CRCs and En PCD enclaves.

the rims is indicative of a progressive re-equilibration with the mafic magma, depending on the interaction time. The groundmass orthopyroxene of the PCD enclaves shows values near the equilibrium interval, compatible with crystallization in progressively evolving melt during enclave formation.

A different history is recorded by the orthopyroxene from the CRCs, as also suggested by the compositional behavior described in Sect. 4.3.2. It displays a large spread in FeO/MgO $_{mol}$, with compositions shifting from equilibrium (only a few crystals) towards high values (up to 0.78). Similar to what is observed for olivine, this relates to a relatively rapid crystallization process in a progressively more evolved magma, probably during CRC formation in the UP rhyolites.

Clinopyroxenes provide further complementary evidence for these processes. The two microlites analyzed in the UP pumice (Mg# 0.79-0.80) approach equilibrium composition, whilst clinopyroxenes from PCD lavas (mainly micro-phenocrysts and microlites) show a large spread in their FeO/MgO_{mol} (from 0.15 to 0.4) across equilibrium at both higher and lower values (Fig. 8c). The only two phenocrysts analyzed in the PCD lavas (Mg# 0.71-0.72) have higher Kd_{s/l} than the equilibrium value, indicating crystallization from a more evolved, Fe-rich melt. Similar to what is observed for orthopyroxene, the melt in equilibrium with the phenocrysts would have a high FeO/MgO_{mol}, comparable to that of the UP pumice (as can be inferred from Fig. 8c). This confirms that these phenocrysts started to crystallize in the UP system, forming the same mush cumulates later remobilized within the PCD lavas, as also validated by the similar petrographic characteristics (subhedral crystal aggregates with oxides; see Sect. 4.1). The clinopyroxene of both the CRCs and the PCD enclaves (mainly normally zoned micro-phenocrysts and microlites) depicts the same behavior of olivine and CRC orthopyroxenes and testifies to rapid crystallization with progressive change in the melt composition, as also demonstrated by the high FeO/MgO_{mol} of the groundmass. Overall, it is striking that the whole FeO/MgO_{mol} range observed in clinopyroxene micro-phenocrysts and microlites in the PCD lavas perfectly corresponds to that of the CRCs and PCD enclaves, indicating that they originated in the mafic melts forming enclaves and later disaggregated into the host.

The evaluation of the equilibrium demonstrates that the large compositional variability recorded by the femic phases, especially pyroxenes, is acquired during crystallization from different melts at different stages of the UP–PCD transition within a dynamic, rapidly changing magmatic environment. These findings can be summarized as follows:

i. The bulk rocks of UP pumice and PCD lavas (used as representative of the liquid composition) always have less evolved compositions than those expected from mineral equilibria. This is due to the presence of dispersed and disaggregated micro-enclaves (e.g.,

- Humphreys et al., 2009) that increase with time during PCD activity (Fig. 8).
- ii. Orthopyroxene and clinopyroxene phenocrysts crystallized in the UP system, progressively forming a crystal mush cumulate that was later remobilized into the PCD lavas, similar to what was already observed for plagioclase phenocrysts by Braschi et al. (2014).
- iii. Clinopyroxene microlites and the groundmass of the CRCs and enclaves indicate rapid crystallization due to the fast cooling of the evolving enclave-forming magma during interaction with the evolved host magma.
- iv. Orthopyroxenes of CRCs and PCD enclaves show distinct behavior. In the CRCs, orthopyroxene represents the principal phase that crystallizes within the evolving mafic melt, frequently together with clinopyroxene, with which it forms intergrowing aggregates (Sect. 5.2, Fig. S4a). In the PCD enclaves, orthopyroxene occurs mainly as xenocrysts entrained from the evolved host and crystallizes only as the groundmass at a later stage of the enclaves' formation. Such a difference can be related not only to the different compositions and degrees of evolution but also to the different cooling paths of the mafic-magma-forming CRCs and PCD enclaves favoring orthopyroxene stability (e.g., Lindsley, 1983; Krawczynski et al., 2012).

This evidence argues for different physico-chemical conditions in the two mafic systems feeding the evolved reservoir during the two phases of activity.

5.2 Evidence from the application of geothermobarometers

Mineral compositions can be used to constrain the crystallization conditions. In the previous section, we highlighted the heterogeneous composition of all the analyzed phases within Nisyros products, revealing a complex history and resulting in evident disequilibrium between minerals and melts. This is a common feature of volcanic systems characterized by interaction and mingling of different magmas (e.g., Browne et al., 2006; Humphreys et al., 2006, 2009; Landi et al., 2019), and it represents a major problem for the application of geothermobarometers based on crystal-liquid thermodynamic equilibria (e.g., Putirka, 2008, 2016). We thus apply a different approach compared to previous studies (i.e., Klaver et al., 2017; Popa et al., 2019) based on a careful and detailed selection of appropriate mineral phases. We particularly consider the mafic products (CRCs and PCD enclaves) and not only the evolved host (as is usually done by, for example, Bachmann et al., 2012, and Popa et al., 2019), because, despite the former showing a rapid evolution of their mineral phases (Sect. 5.1), they better retain the original information with respect to the latter contrast, which instead displays evident mixed/mingled features.

Recent advancements in thermobarometry are indeed driven by the application of single-crystal machine learning techniques, which are producing a significant methodological shift by providing reliable predictions of P–T conditions of magma storage and migration, and are poised to set the basis for a novel generation of thermobarometers extending beyond the paradigm associated with crystal-liquid equilibrium (e.g., Petrelli et al., 2020; Higgins et al., 2022; Chicchi et al., 2023). Most of these methods focused on clinopyroxene thermobarometry (e.g., Petrelli et al., 2020; Higgins et al., 2022; Chicchi et al., 2023) and subordinately on amphiboles (e.g., Higgins et al., 2022). In the case of Nisyros volcano, clinopyroxenes and amphiboles can be used to constrain the crystallization conditions of CRCs and PCD enclaves, which, as previously demonstrated, crystallized from mafic magmas rapidly cooled during the interaction with the evolved host. Therefore, the pressure estimations of CRCs and PCD enclaves can be considered to be the same as their respective host magma reservoirs. In particular, they identify the pressure conditions of the levels where mafic and evolved melts interacted prior to eruption.

Hereafter, we describe and discuss the P–T conditions obtained from such mafic phases (e.g., Higgins et al., 2022; Chicchi et al., 2023), integrating the results with estimates of temperatures, water content, and redox conditions of the host lavas based on plagioclase and Fe–Ti oxides (Putirka, 2008; Lepage, 2003) (Fig. 9, Table S5).

The results are shown in Fig. 9 and indicate a large P interval between 0.5 and 7 kbar. According to the Chicchi et al. (2023) geobarometer, clinopyroxenes from the UP system (mostly CRCs) cluster between 0.5 and 1 kbar, with a few scattered higher pressures up to 7 kbar (Fig. 9a). The high pressures are recorded in the cores of zoned microphenocrysts of a Type-C CRC with the highest Mg# (Figs. 6 and S5) and can be considered an early crystallization in a deeper level of the plumbing system, before ascent in the shallow crust.

Clinopyroxene of the PCD system yields more variable pressures but no clear distinction between PCD host lavas and enclaves (Fig. 9b-c). This overlapping is perfectly consistent with the origin of clinopyroxene through disaggregation of the enclaves and dispersion into the host (see previous paragraph). Within PCD enclaves, two broad clusters can be identified at < 1 kbar and 2.5–3.5 kbar. This is particularly evident in the enclaves of the older domes, whilst those from the younger ones yield a single peak around 3 kbar (Fig. 9b, c). In PCD host lavas, the two clusters are barely visible in the older domes, where low pressures predominate, but not in the younger ones, showing a broadly continuous distribution. The slightly different pressure distribution between the older and younger PCD host lavas provides further evidence that enclave disaggregation processes increase with time during the PCD activity, randomly redistributing crystals originated at different pressures. A few crystals at high pressure (> 5 kbar) were also found in both PCD host lavas and enclaves.

The clinopyroxene thermobarometer of Higgins et al. (2022) provides a single range of pressure, from 1.5 to 8 kbar, but does not clearly highlight the presence of specific clusters. Moreover, it does not yield any pressure below 1.5 kbar, which is instead detected by the Chicchi et al. (2023) method. This is likely due to the larger predicted errors (and SEE) returned by the Higgins et al. (2022) algorithm (1.8 kbar on average) compared to those (0.5 kbar on average) calculated by Chicchi et al. (2023). Accordingly, for clinopyroxene, only the pressures calculated with the method of Chicchi et al. (2023) is used for the following discussion.

The Higgins et al. (2022) geothermobarometer can also be applied to amphiboles (Fig. 9d), providing a further independent constraint. In this case, the method of Higgins et al. (2022) represents the only available alternative to Ridolfi (2021), also providing slightly lower predicted errors (1.2 kbar on average) and SEE compared to the clinopyroxene method. Interestingly, the pressures calculated on amphiboles broadly confirm the range estimated from clinopyroxenes and similarly identify the distinction between CRCs at lower P clustering around 2 kbar and PCD enclaves showing a large range from 2 to 7 kbar with a peak around 5 kbar. Similar results are obtained using the method of Ridolfi (2021) (Fig. 9d). Notably, as for clinopyroxene, the results obtained by Higgins et al. (2022) buffer around 2 kbar with no records of lower pressures; moreover, they do not detect the two P clusters for the PCD system.

Overall, combining the evidence from pressure estimates on both clinopyroxene and amphiboles and referring in particular to the results of Chicchi et al. (2023), we can suggest the presence of two main storage levels during this phase of activity of the Nisyros volcano. The UP eruption was fed by the shallower reservoir, where the mingling processes responsible for the formation of the CRCs took place. The PCD activity was, in contrast, fed by both the same shallow reservoir and a deeper one. Here the interaction between mafic and evolved melts occurred at all levels. The younger PCD enclaves indicate that the interaction occurred mostly at deeper levels than in the older ones, suggesting a change in the main localization of the interaction horizon with time.

Temperature results provide information on the thermal conditions of the mafic magmas. In particular, the highest values indicate the initial temperatures of the mafic inputs intruding into the evolved reservoir/s.

The estimations obtained in clinopyroxene by Chicchi et al. (2023) provide values between 1050 and 1150 °C for CRCs (clustering at 1100 °C) and from 1000 to 1180 °C for PCD enclaves. The algorithm of Higgins et al. (2022) for clinopyroxene returns similar ranges, with slightly lower estimated temperature only for the UP system. Amphibole indicates generally lower temperatures than clinopyroxene (820–1000 °C, Higgins et al., 2022) and clearly discriminates between CRCs and PCD enclaves (Fig. 9d): the former reach

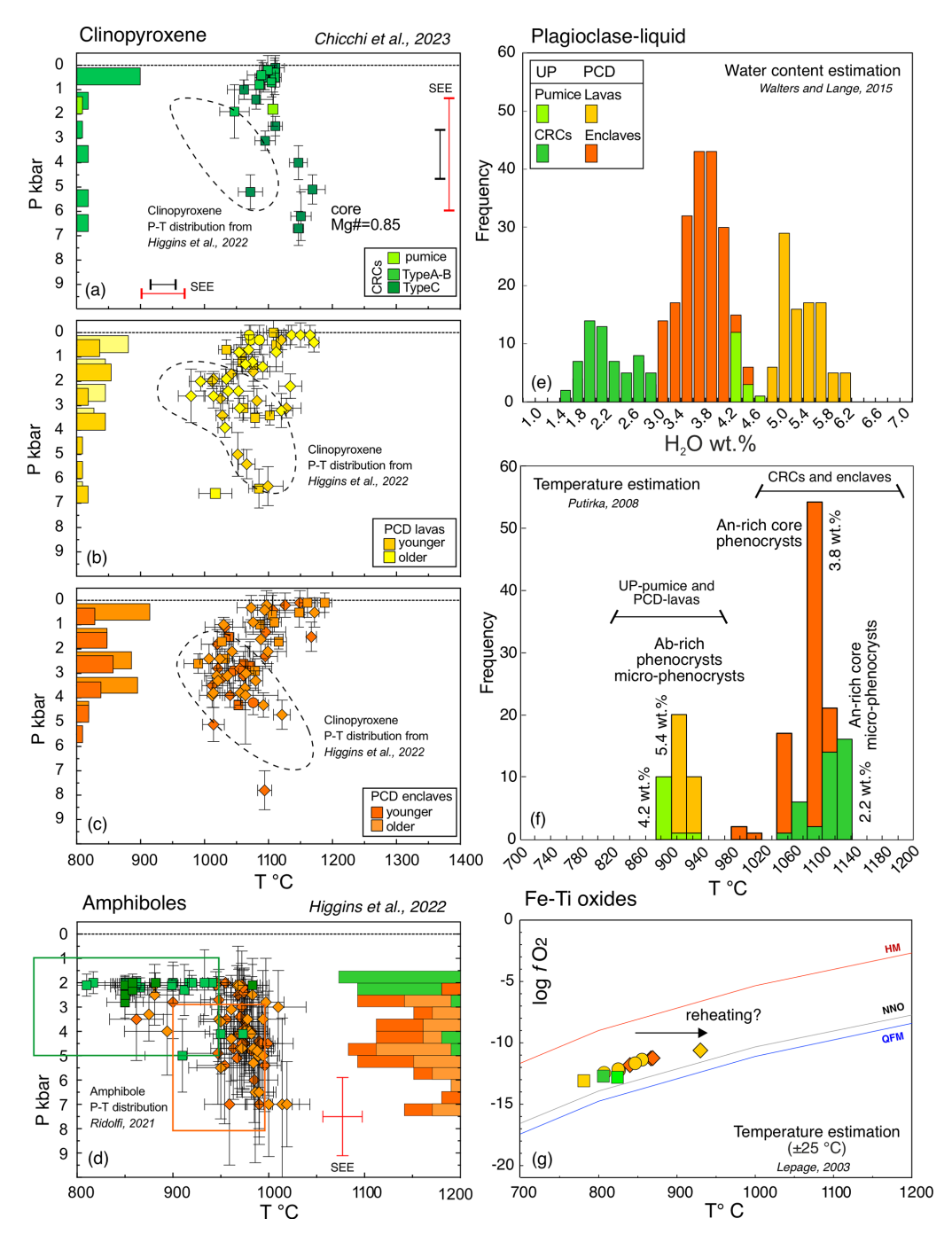


Figure 9. Overview of the geothermobarometer results obtained by the machine learning methods of Chicchi et al. (2023) on clinopyroxenes (**a–c**) and Higgins et al. (2022) on amphiboles (**d**) (Tables S3–S4). Histograms on the *y* axes indicate the statistical distribution of the data density clouds on pressures. Predicted errors on pressure and temperature are shown by symbol bars and reported in Table S3. The standard error estimate (SEE) is also shown. It provides the performance of the models and measures the ability of the algorithm to predict the testing datasets. The 1 SEE of Chicchi et al. (2023) is 1 kbar and 30 °C for P and T (black bars in plot **a** for graphical reference); the 1 SEE of Higgins et al. (2022) is 2.3 kbar and 57 °C for clinopyroxene and 1.6 kbar and 40 °C for amphiboles (red bars in plot **a** for graphical reference). Within plots (**a–c**), the dashed fields represent the more representative P–T interval obtained by the application of the Higgins et al. (2022) method. For comparison, in plot (**d**), the green and orange boxes represent the P–T range obtained by the application of the Ridolfi (2021) method. Plot (**e**) shows the results from the plagioclase hygrometer of Waters and Lange (2015). Temperature estimates from the plagioclase–liquid thermometer of Putirka (2008) and the Fe–Ti oxide thermometer along with oxygen fugacity (fO₂) of Lepage (2003) are also shown in plots (**f**) and (**g**), respectively, comparing the UP pumice and PCD lavas to CRCs and PCD enclaves. For the plagioclase–liquid thermometer, the required water content is estimated from the plagioclase–liquid hygrometry of Waters and Lange (2015) and pressure from Chicchi et al. (2023). Symbols and colors are the same as in Figs. 7 and 8.

lower and variable values, mainly around 850 °C, whereas the latter provide more homogeneous temperature clustering at 980 °C. Temperature estimation on amphibole was also tested using the method of Ridolfi (2021) for comparison (Fig. 9d). This method is not fully appropriate for application to amphiboles formed by the process of quenching, but the general agreement of the P–T distribution is considered to further corroborate the evidence of two distinct behaviors between UP and PCD systems.

In order to understand the different temperature intervals yielded by clinopyroxene and amphibole and the difference between the temperature of CRCs and PCD enclaves, the crystallization conditions of the two mineral phases and their stability within the two mafic melts should be deciphered, especially considering the effect of water content.

The water content of the different products has been determined using the hygrometer (Fig. 9e) of Waters and Lange (2015). For the mafic products, results show lower values in the CRCs compared to PCD enclaves (2.2 wt % and 3.8 wt %, respectively). First of all, this evidence can explain the general temperature overlap of the CRCs and PCD enclaves, which seems to be in contrast with the higher degree of evolution of CRC products (and the lower Mg# of clinopyroxene) compared to the PCD enclaves. The lower water content of the CRC samples compared to PCD enclaves indeed allows clinopyroxene crystallization at high temperatures, thus providing similar T values.

Further, the higher T obtained by clinopyroxene compared to amphibole suggests that clinopyroxene started to crystallize first, probably during the initial intrusion of the mafic melt into the host, both for CRCs and PCD enclaves (Fig. 10a). Later, as temperature decreases, the balance between T and H₂O content reaches a suitable condition for amphibole crystallization (e.g., Krawczynski et al., 2012). This step occurs differently in CRCs and PCD enclaves, as also suggested by the distinct compositional behavior of amphiboles described in Sect. 4.3.4. In CRCs, the lower water content (Fig. 9e) allows amphibole crystallization at lower T than in PCD enclaves. This cooling step is relatively slow to allow the T-sensitive Al and Ti elements to record a progressive variation in amphibole composition (Figs. 7d and S7a) that consequently records the observed large spread in temperature. In contrast, the PCD enclaves, having a higher water content, start to crystallize amphiboles at higher T; this, combined with the efficient T contrast with the host, generates rapid, massive crystallization, as suggested by the more homogeneous compositions of amphiboles from the PCD enclaves compared to those from CRCs (Figs. 7d and S7a), and is consistent with their petrographic characteristics (Sect. 4.2).

The role and composition of plagioclase are also dependent on the T– H_2O relationships and on the magma composition (Sisson and Grove, 1993; Bennett et al., 2019). In the PCD enclaves, the crystallization of anorthite-rich plagioclases (An_{85-95} , Fig. 7c) was favored in an initial stage

(Fig. 10a), probably before the intrusion into the rhyolitic host when amphibole became stable (Pichavant and Macdonald, 2007; Krawczynski et al., 2012), progressively decreasing the water content in the mafic melt. This, together with the rapid T drop (due to the magma undercooling related to the contact with the host), favored the stabilization of less calcic plagioclases (An_{65–80}, Fig. 7c) that formed the groundmass crystal network together with amphiboles (Fig. 10a). Conversely, in the CRCs, the lower water content allowed plagioclase (An_{65–90}, Fig. 7a) crystallization at slightly higher temperatures (Fig. 9f), together with pyroxene, until amphibole became stable (Fig. 10a).

This behavior is in good agreement with the compositional pattern of the clinopyroxene in PCD enclaves (Sect. 4.3.3), showing progressive enrichment in the Al content (Fig. S6c), until amphibole and plagioclase become stable. When these two phases crystallize massively, clinopyroxene is indeed suppressed, in turn favoring orthopyroxene stability as microlites in the last stage of crystallization (Fig. 10a).

The thermal conditions of the evolved host magmas can only be evaluated by the thermodynamic-based thermometer of Putirka (2008) on plagioclase or by an Fe–Ti oxide thermometer. For the same reason explained in the previous paragraph, we use the whole-rock compositions as representative of the liquid, and we compare them to the core composition of low-An plagioclases. These plagioclase crystals are coherently expected to crystallize from evolved liquids, such those of the UP pumice and PCD lavas.

The plagioclase-liquid pairs yield similar temperatures for the two evolved melts, with UP depicting slightly lower values, at 880 °C, compared to PCD, at 900-920 °C (Fig. 9f). Fe-Ti oxides yield slightly lower values (Fig. 9g), with UP at 820 °C and PCD ranging between 780-940 °C (with an average value at 850°). In this case, the high T value is recorded by a microlite pair, whereas the other values are provided by phenocryst and micro-phenocryst pairs in aggregate with orthopyroxene. The obtained plagioclase-liquid temperatures appear generally higher than those expected for a rhyolitic system in a pre-recharge storage stage (e.g., Popa et al., 2019). In this regard, it is remarkable that, for the PCD lavas, the bulk composition of the magma became progressively more mafic due to the mingling/mixing with the mafic refilling melts (Braschi et al., 2012). The plagioclase-liquid pairs that satisfy the Putirka (2008) equilibrium boundaries thus return a temperature that is affected by this hot re-input. In light of this, the estimated temperatures reflect a reheated, post-recharge environment (mainly affecting the PCD), as also revealed by the evident resorbed textures of plagioclase (but also pyroxene) phenocrysts and micro-phenocrysts and by the higher temperature of the microlite oxide pair (Fig. 9g). The obtained temperatures are, however, at least 150 °C lower than those found for CRCs and PCD enclaves. This difference is enough to produce a suitable thermal contrast, promoting immiscibility and quenching in both the UP and the PCD systems. The slightly higher temperature of the PCD lavas probably reflects major reheating of the whole PCD system due to repeated mafic magma refilling after the *post-UP* stage between the two eruptive phases (Braschi et al., 2012).

In the UP, the interaction between CRCs and the rhyolitic host is thus rapid, with negligible reheating of the evolved host, as also confirmed by the euhedral shape of the plagioclase cargo and the homogeneous composition of the host magmas (Fig. S1). In this regard, it is worth stressing that the compositional (and textural) bimodality observed in the PCD plagioclases (Sect. 4.3.4) is not present in the UP. This indicates that the crystal exchange process between the host pumice and the mafic-intruding melt was limited in the UP system, thus strengthening the evidence of a short interaction interval before eruption.

In the PCD, the reheating induced by the hot, mafic, and H₂O-richer magmas forming the enclaves primed a perturbation in the evolved colder host magma, allowing mush cumulate remobilization and promoting interactions between the two melts over longer timescales with respect to UP, hence providing the required conditions to induce the effusive eruption. In this light, the high H₂O content of the PCD lavas (up to 6.2 wt %, with a mode around 5.6 wt %, Fig. 9e) coincides with the water saturation limit between 5.5 wt % and 6 wt % H₂O constrained by Popa et al. (2019, 2021a, b) for the evolved melts produced at Nisyros-Yali. Therefore, the PCD lavas can be assumed in water-supersaturated conditions (Locher et al., 2025), whilst this is not true for the UP pumice (having H₂O at 4.2 wt %-4.6 wt %). These authors suggest that the presence of high exsolved water in storage conditions increases the bulk compressibility of the stored magma body, hence allowing it to better accommodate the volume of recharge material before erupting, promoting more efficient reheating and thus a larger viscosity drop in the silicate melt (e.g., Degruyter et al., 2017). As a result, in contrast to what could be expected, the higher H₂O content of PCD lavas with respect to UP would favor their effusive eruption. It should also be considered that the water solubility in magmas strongly increases with increasing P (e.g., Liu et al., 2005) and counterbalances the effect of a possible T increase. Consequently, the general deeper storage level estimated for PCD with respect to the UP can explain the higher H₂O content found in the former, even if at slightly higher T. The combination between the higher P storage and lower viscosity of the reheated host magma may favor efficient outgassing during magma ascent (e.g., Popa et al., 2021b), thus promoting the effusive eruptive style of PCD.

Further, due to the efficient reheating, the thermal conditions of the PCD lavas did not allow crystallization but instead promoted remelting (i.e., plagioclase phenocrysts are all subhedral with rounded shapes, Fig. 3g). Microlites and groundmass, in contrast, formed later, probably during magma ascent and emplacement (Fig. 10a). In the effusive phase, the ascent rate and the post-emplaced cooling are in-

deed slower than in the explosive event, allowing late crystallization.

5.3 Plumbing system evolution

Based on plagioclase mineralogy and in situ isotopes, we already postulate that the PCD inherited the same magma chamber of the UP due to the strict correspondence between the main composition and Sr isotopic signature of phenocrysts hosted in the two systems (Braschi et al., 2012, 2014). In this work, however, new data mainly based on mafic phases provide further elements, indicating an even more complex picture (Fig. 10b). Indeed, the pressure setting of the evolved UP and PCD reservoirs and, in particular, the interaction horizon with the refilling mafic magmas changed, with a deepening in the final PCD stage.

From the results of the thermobarometers on clinopyroxene and amphibole, the eruptible reservoir of the UP explosive eruption can be identified as a shallow evolved melt-rich magma chamber (Fig. 10b-1). This reservoir was fed shortly before the eruption by heterogeneous mafic batches, which had previously differentiated in multiple, slightly deeper ephemeral reservoirs (Braschi et al., 2022). In the modern view of volcanic settings, shallow lenses of evolved magmas are thought to form through progressive accumulation of evolved melts that segregate from a deeper reservoir (i.e., Annen et al., 2006; Cashman et al., 2017; Ruprecht et al., 2020; Sparks et al., 2022, 2024; Booth et al., 2024). In the UP, the presence of a low amount of plagioclase and orthopyroxene phenocrysts in the erupted pumice may suggest that these crystals represent part of the crystal cargo brought up into the shallower level during segregation from a lower, still relatively evolved reservoir, in which the main differentiation processes occur. This reservoir was hidden at this stage (i.e., it is not recorded by our data) because the main mafic phases used for thermobarometric estimations belong to the mafic magma that directly refilled the shallower chamber. We can imagine, however, that a deeper, evolved reservoir already existed and was probably fractionating during this phase. In our scenario, the mafic refilling is represented by CRCs that intruded directly into the shallower evolved reservoir, mingled with the host, and finally erupted (see Fig. 12 in Braschi et al., 2022, for details). The possibility of finding multiple independent pathways to reach this shallow reservoir, despite the presence of a deeper magma chamber, is far from being demonstrated by this study. We can only observe that, in general, tectonic structures, either pre-existing or newly formed, form complex networks which may allow mafic melts to ascend across the crust along alternative paths (e.g., Maestrelli et al., 2024). After the UP eruption, a relatively long period of volcanic inactivity (possibly 20–30 kyr) led to the establishment of a post-UP stage where the magma left in the crustal reservoirs continues to evolve, increasing the mushy cumulate volume (mainly made up by plagioclase and pyroxenes).

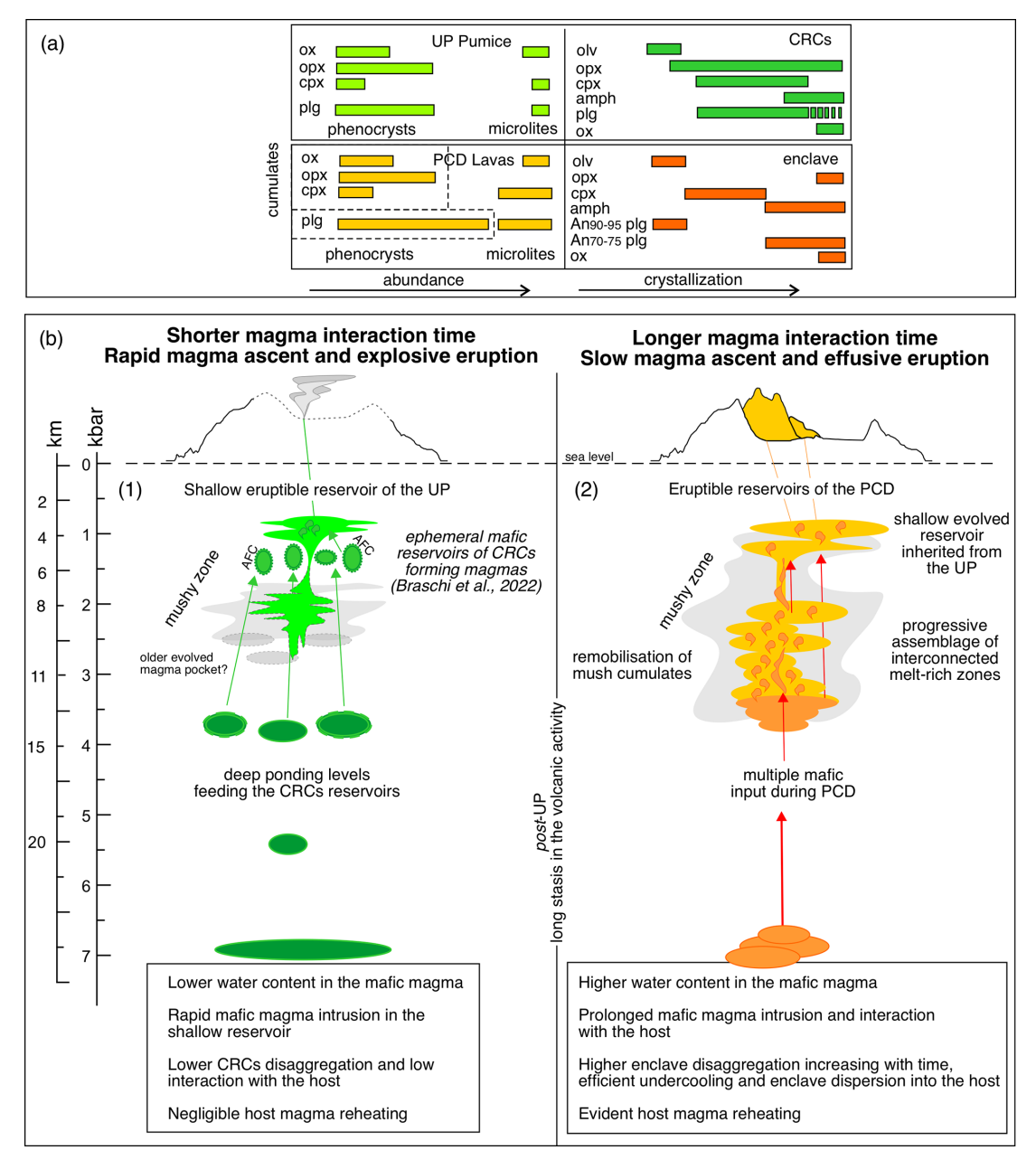


Figure 10. (a) Schematic sketch illustrating the mineral assemblage of the UP pumice and PCD lavas compared to that of the CRCs and PCD enclaves. For the UP pumice and PCD lavas, the length of the bars for each mineral phase is proportional to their abundance (as indicated by the arrow). For the CRCs and PCD enclaves, the length of the bars is instead proportional to the crystallization interval during mafic melt cooling (as indicated by the arrow). Between the CRCs and PCD enclaves, the crystallization order and the competition between the different minerals clearly change according to the different evolutionary degrees of the mafic magmas and the different phase stability during undercooling and enclave formation. (b) Schematic sketch of the evolution of the plumbing system from the UP (b-1) to the PCD (b-2) activity (colors as in panel a), highlighting the changes in the plumbing system structure and summarizing the main findings on magma characteristics and interaction dynamics.

The important evidence, however, is that during the successive PCD phase (Fig. 10b-2), the plumbing system dynamics changed, and the erupted products reveal the coexistence of two main reservoirs at different levels, which were both involved in the eruptions and thus both provided

eruptible melts. In the PCD phase, the shallower and deeper evolved reservoirs are both inherited from the UP and further developed during the *post-UP* stage into a more vertically extended system possibly made of interconnected meltrich lenses (Fig. 10b-2). The new inputs of mafic magmas

then refilled and reactivated the whole evolved system, together with their cumulates, providing heat and volatiles to the system. These dynamics have been described in detail by Braschi et al. (2012) and agree well with the obtained P-T results, also highlighting further evolution of the interaction within the PCD. The interaction between the mafic inputs and the evolved host indeed decreased in the shallow reservoir with time (i.e., from the older to the younger PCD) and instead concentrated at higher depths in the deeper reservoir. The shallow reservoir still actively fed the PCD eruption and is directly refilled from below (Fig. 10b-2), but the deeper one became the prevalent level at which the interaction processes generating enclaves occurred. This implies that, during the PCD stage, the multiple refilling mafic magmas preferentially intruded at higher depths, increasing their volume at the base of the deeper magma chamber and leading to a slight ascent of the interaction level (i.e., Fig. 12 in Braschi et al., 2012), as testified by the prevalent P values characterizing the younger PCD enclaves. This mechanism contributes to the generation of a more mafic signature of the erupted products with time.

The obtained results provide interesting evidence of a remodeling of the magmatic feeding system at Nisyros during the transition period between the UP and PCD stage. The recent dating of PCD confirms a period of quiescence of at least 30 kyr between the two activities (Locher et al., 2025), in which the plumbing system developed into a deeper setting, generating a more complex, vertical system of interconnected melt lenses.

On the whole, our findings show that the evolved system persisted from the UP to the PCD period, but the main active (i.e., eruptible/involved in the eruption) reservoir was relocated at a deeper level. This can possibly be related to the structural perturbations which follow caldera collapses (e.g., Kennedy et al., 2018). Previous works (e.g., Tibaldi et al., 2008) have indeed suggested complex interplays between the regional tectonic setting and the local stress regime, which is in turn controlled by inflation/deflation episodes related to the evolution of the Nisyros volcanic system.

Further, we also provide evidence of a clear change in the refilling mafic magma composition and in the interaction dynamics with the evolved host, associated with a variation in the general P–T conditions between the two volcanic phases. The different conditions of magmatic supersaturation in H₂O of the evolved reservoirs, from UP to PCD systems, were recognized as the main factor controlling the shift from explosive to effusive activity (Popa et al., 2019, 2021b). However, we suggest that the establishment of a more vertically extended and highly dynamic storage system in the PCD stage (Fig. 10b), favored by the prolonged mafic intrusions during the transition period between UP and PCD and associated with the change in the characteristics of the mafic refilling magma, represents a fundamental factor that may have promoted this shift. The CRC-forming magma indeed has a more evolved composition than that of the PCD enclaves, and it differentiated through AFC at crustal levels (Fig. 10b-1), also involving deep assimilation of carbonate lithologies, before intruding into the shallow evolved magma chamber (Braschi et al., 2022). This may have induced higher CO₂ contents (and less H₂O) in the CRCs compared to the PCD enclaves, providing another critical factor favoring the explosive style of the UP eruption (e.g., Buono et al., 2020; Chadwick et al., 2007).

An additional alternative or concurrent process that could influence the eruption style and the transition from explosive to effusive eruptions is related to tectonics and to the effects of possible changes in regional/local extension dynamics and stress regimes (e.g., Acocella et al., 2015). This may indeed influence the plumbing system dynamics or magma stagnation levels, as well as the fluxes of primitive melts rising from deep magma reservoirs (e.g., Hutchison et al., 2016).

6 Conclusions

The detailed comparison of the mineral chemistry characteristics of the juvenile products erupted during the two more recent volcanic events on Nisyros volcano (UP explosive and PCD effusive eruptions), coupled with thermobarometric estimations, has provided valuable evidence for the reconstruction of the magmatic feeding system architecture and its evolution during these two periods of activity.

We have demonstrated that a crystal/liquid disequilibrium condition is a common and widespread process occurring in these long-lived, multiple refilled systems and that the application to these systems of the geothermobarometers using mineral/melt equilibrium could be critical.

Our results have also pointed out a change in the general assessment of magma accumulation during the significant quiescence stage of Nisyros volcano (at least 30 kyr), marking the transition period from the caldera-forming explosive UP to the effusive PCD activity. This period allowed the build-up of a multiple-storage magmatic system, sustained by the intrusion of mantle-derived basalt.

Through mineral investigations, we have also provided insights into the history and interaction dynamics of magmas with different differentiation degrees, which point to a more stirred system in the pre-eruptive period of the effusive phase. Such evolution is consistent with magma storage existing for a protracted time, supporting the hypothesis of long-lasting, persistent magma storage above the solidus (i.e., Szymanowski et al., 2017; Laumonier et al., 2019), even beneath relatively small volcanoes such as Nisyros. The proposed reconstructed evolution of a polybaric system made up by multiple crustal pounding levels may contribute to the knowledge of the behavior of silicic, composite volcanoes with cyclic eruptive styles and periodic mafic refilling, providing elements to define the boundary conditions of magma storage. In fact, this study suggests that the characteristics of

the refilling mafic magma may also play a role in determining the eruptive behavior of evolved bodies stored in the crust.

We finally point out that the careful study and interpretation of the history of each mineral phase is fundamental for investigating magmatic systems characterized by interactions between different melts through pervasive and widespread (mechanical) mingling.

Data availability. Mineral chemistry data of Post Caldera Domes samples reported in this article are available in the Supplement (Table S2). Mineral compositions of Upper Pumice samples are available at https://ecl.earthchem.org/view.php?id=2230 (last access: 1 October 2025).

Supplement. The supplement related to this article is available online at https://doi.org/10.5194/ejm-37-793-2025-supplement.

Author contributions. EB: fieldwork and sampling, writing – original draft, supervision, methodology, analysis, data curation, conceptualization, editing, and discussion. FG: analysis, initial conceptualization. FM: analysis. AO: analysis, discussion. RA: writing, editing, discussion. ST: discussion, initial conceptualization. GEV: fieldwork and sampling, discussion. LF: fieldwork and sampling, writing, supervision, conceptualization, editing, and discussion.

Competing interests. The contact author has declared that none of the authors has any competing interests.

Disclaimer. Publisher's note: Copernicus Publications remains neutral with regard to jurisdictional claims made in the text, published maps, institutional affiliations, or any other geographical representation in this paper. While Copernicus Publications makes every effort to include appropriate place names, the final responsibility lies with the authors.

Special issue statement. This article is part of the special issue "Celebrating the outstanding contribution of Paola Bonazzi to mineralogy". It is not associated with a conference.

Acknowledgements. This paper is dedicated to the memory of Paola Bonazzi, who sadly passed away last year. Lorella Francalanci shared many years of work with Paola in their department, and with this article she wants to remember her love for minerals. The paper is the result of several contributions acquired in the years after Eleonora Braschi's PhD and benefits from discussions made by the authors during the master's theses of Filippo Mastroianni and Francesca Giannetti. Chiara Maria Petrone is particularly thanked for helping with the EPMA analyses during Eleonora Braschi's PhD thesis. Giacomo Corti is acknowledged for his valuable help in sharing his point of view regarding volcano—tectonic processes and their implications. We would like to thank Dejan Prelević and Elis-

abetta Rampone for the editorial handling. Laurent Arbaret, Diego González-García, and Joan Andujar are also warmly thanked for their suggestions and critical reviews that greatly helped to improve the paper.

Financial support. Financial support was provided by the Italian MIUR through the PRIN-2017 funding grant 20178LPCPW, issued to Lorella Francalanci by the University of Florence through a PhD grant to Eleonora Braschi in 2006–2008 and by the PNRR Return – Multi-risk science for resilient communities under a changing climate project, funded by the European Union's NextGenerationEU.

Review statement. This paper was edited by Dejan Prelevic and reviewed by Laurent Arbaret, Joan Andujar, and Diego González-García.

References

Acocella, V., Di Lorenzo, R., Newhall, C., and Scandone, R.: An overview of recent (1988 to 2014) caldera unrest: Knowledge and perspectives, Rev. Geophys., 53, 896–955, 2015.

Anderson, T., O'Reilly, S. Y., and Griffin, W. L.: The trapped fluid phase in upper mantle xenoliths from Victoria, Australia: Implications for mantle metasomatism, Contrib. Mineral. Petr., 115, 505–514, 1984.

Annen, C., Blundy, J. D., and Sparks, R. S. J.: The genesis of intermediate and silicic magmas in deep crustal hot zones, J. Petrol., 47, 505–539, https://doi.org/10.1093/petrology/egi084, 2006.

Bacon, C. R.: Magmatic inclusions in silicic and intermediate volcanic rocks, J. Geophys. Res., 91, 6091, https://doi.org/10.1029/JB091iB06p06091, 1986.

Bacon, C. R. and Metz, J.: Magmatic inclusions in rhyolites, contaminated basalts, and compositional zonation beneath the Coso volcanic field, California, Contrib. Mineral. Petr., 85, 346–365, https://doi.org/10.1007/BF01150292, 1984.

Bachmann, O., Charlier, B. L. A., and Lowenstern, J. B.: Zircon crystallization and recycling in the magma chamber of the rhyolitic Kos Plateau Tuff (Aegean arc), Geology, 35, 73–76, https://doi.org/10.1130/G23151A.1, 2007.

Bachmann, O., Deering, C. D., Ruprecht, J. S., Huber, C., Skopelitis, A., and Schnyder, C.: Evolution of silicic magmas in the Kos-Nisyros volcanic center, Greece: a petrological cycle associated with caldera collapse, Contrib. Mineral. Petr., 163, 151–166, https://doi.org/10.1007/s00410-011-0663-y, 2012.

Barberi, F., Navarro, J. M., Rosi, M., Santacroce, R., and Sbrana, A.: Explosive interaction of magma with ground water: insights from xenoliths and geothermal drillings, Rend. Soc. Ital. Mineral. Petrol., 43, 901–926, 1988.

Bennett, E. N., Lissenberg, C. J., and Cashman, K. V.: The significance of plagioclase textures in mid-ocean ridge basalt (Gakkel Ridge, Arctic Ocean), Contrib. Mineral. Petr., 174, 1–22, https://doi.org/10.1007/s00410-019-1587-1, 2019.

Blake, S. and Fink, J. H.: On the deformation and freezing of enclaves during magma mixing, J. Volcanol. Geotherm. Res., 95, 1–8, https://doi.org/10.1016/S0377-0273(99)00129-8, 2000.

- Booth, C., Jackson, M., Sparks, S., and Rust, A.: Magma Storage, Differentiation and Transfer in Vertically Extensive Magmatic Systems, EGU General Assembly 2024, Vienna, Austria, 14–19 Apr 2024, EGU24-11344, https://doi.org/10.5194/egusphere-egu24-11344, 2024.
- Braschi, E., Francalanci, L., and Vougioukalakis, G. E.: Inverse differentiation pathway by multiple mafic magma refilling in the last magmatic activity of Nisyros Volcano, Greece, Bull. Volcanol., 74, 1083–1100, https://doi.org/10.1007/s00445-012-0585-1, 2012.
- Braschi, E., Francalanci, L., Tommasini, S., and Vougioukalakis, G. E.: Unraveling the hidden origin and migration of plagioclase phenocrysts by in situ Sr isotopes: the case of final dome activity at Nisyros volcano, Greece, Contrib. Mineral. Petr., 167, 1–25, https://doi.org/10.1007/s00410-014-0988-4, 2014.
- Braschi, E., Mstroianni, F., Di Salvo, S., Casalini, M., Agostini, S., Vougioukalakis, G. E., and Francalanci, L.: Unveiling the occurrence of transient, multi-contaminated mafic magmas inside a rhyolitic reservoir feeding an explosive eruption (Nisyros, Greece), Lithos, 410–411, 106574, https://doi.org/10.1016/j.lithos.2021.106574, 2022.
- Browne, B. L., Eichembergere, J. C., Patino, L. C., Vogel, T. A., Dehen, J., Uto, K., and Hoshizumi, H.: Generation of Porphyritic and Equigranular Mafic Enclaves During Magma Recharge Events at Unzen Volcano, Japan, J. Petrol., 47, 301–328, https://doi.org/10.1093/petrology/egi076, 2006.
- Buettner, A., Kleinhanns, I. C., Rufer, D., Hunziker, J. C., and Villa, I. M.: Magma generation at the easternmost section of the Hellenic arc: Hf, Nd, Pb and Sr isotope geochemistry of Nisyros and Yali volcanoes (Greece), Lithos, 83, 29–46, https://doi.org/10.1016/j.lithos.2005.01.001, 2005.
- Buono, G., Pappalardo, L., Harris, C., Edwards, B. R., and Petrosino, P.: Magmatic stoping during the caldera-forming Pomici di Base erutpion (Somma-Vesuvius, Italy) as a fuel of eruption explosivity, Lithos, 370–371, 105628, https://doi.org/10.1016/j.lithos.2020.105628, 2020.
- Cashman, C. V. and Giordano, G.: Calderas and magma reservoirs, J. Volcanol. Geotherm. Res., 288, 28–45, https://doi.org/10.1016/j.jvolgeores.2014.09.007, 2014.
- Cashman, K. V., Sparks, R. S. J., and Blundy, J. D.: Vertically extensive and unstable magmatic systems: a unified view of igneous processes, Science, 355, eaag3055, https://doi.org/10.1126/science.aag3055, 2017.
- Chadwick, J. P., Troll, V. R., Ginibre, C., Morgan, D., Gertisser, R., Waight, T. E., and Davidson, J. P.: Carbonate Assimilation at Merapi Volcano, Java, Indonesia: insights from crystal isotope stratigraphy, J. Petrol., 48, 1793–1812, https://doi.org/10.1093/petrology/egm038, 2007.
- Chicchi, L., Bindi, L., Fanelli, D., and Tommasini, S.: Frontiers of thermobarometry: GAIA, a novel Deep Learning-based tool for volcano plumbing systems, Earth Planet. Sc. Lett., 620, 118352, https://doi.org/10.1016/j.epsl.2023.118352, 2023.
- Coombs, M. L., Eichelberger, J. C., and Rutherford, M. J.: Experimental and textural constraints on mafic enclave formation in volcanic rocks, J. Volcanol. Geoth. Res., 119, 125–144, 2002.
- Davidson, J. P., Morgan, D. J., Charlier, B. L. A., Harlou, R., and Hora, J. M.: Microsampling and isotopic analysis of igneous rocks: implications for the study of magmatic systems, Annu. Rev. Earth Pl. Sc., 35, 273–311, 2007.

- Davis, E. N.: Zur Geologie und Petrologie der Inseln Nisyros und Jali (Dodekanes), Praktika Akan Athen, 42, 235–252, 1967.
- Degruyter, W., Huber, C., Bachmann, O., Cooper, K. M., and Kent, A. J. R.: Influence of exsolved volatiles on reheating silicic magmas by recharge and consequences for eruptive style at Volcan Quizapu (Chile), Geochem. Geophy. Geosy., 18, 4123–4135, 2017.
- DePaolo, D. J.: Trace element and isotopic effects of combined wallrock assimilation and fractional crystallization, Earth Planet. Sc. Lett., 53, 189–202, https://doi.org/10.1016/0012-821X(81)90153-9, 1981.
- Dietrich, V. J.: Geology of Nisyros Volcano, in: Nisyros Volcano, Active Volcanoes of the World, edited by: Dietrich, V. J. and Lagios, E., https://doi.org/10.1007/978-3-319-55460-0_12, 2018.
- Di Salvo, S., Avanzinelli, R., Isaia, R., Zanetti, A., Druitt, T., and Francalanci, L.: Crystal-mush reactivation by magma recharge: evidence from the Campanian Ignimbrite activity, Campi Flegrei volcanic field, Italy, Lithos, 376–377, 105780, https://doi.org/10.1016/j.lithos.2020.105780, 2020.
- Di Paola, G. M.: Volcanology and petrology of Nisyros island (Dodecanese Greece), Bull. Volcanol., 38, 944–987, 1974.
- Elburg, M., Kamenetsky, V. S., Nikogosian, I., Foden, J., and Sobolev, A. V.: Coexisting High- and Low-Calcium Melts Identified by Mineral and Melt Inclusion Studies of a Subduction-Influenced Syncollisional Magma from South Sulawesi, Indonesia, J. Petrol., 47, 2433–2462, https://doi.org/10.1093/petrology/egl050, 2006.
- Forni, F., Bachmann, O., Mollo, S., De Astis, G., Gelmand, S. G., and Ellis, B. S.: The origin of a zoned ignimbrite: Insights into the Campanian Ignimbrite magma chamber (Campi Flegrei, Italy), Earth Planet. Sc. Lett., 449, 259–271, 2016.
- Francalanci, L., Varekamp, J. C., Vougioukalakis, G. E., Defant, M. J., Innocenti, F., and Manetti, P.: Crystal retention, fractionation and crustal assimilation in a convecting magma chamber, Nisyros volcano, Greece, Bull. Volcanol., 56, 601–620, 1995.
- Francalanci, L., Vougioukalakis, G. E., Perini, G., and Manetti, P.: A west-east traverse along the magmatism of the south Aegean volcanic arc in the light of volcanological, chimica and isotope data, in: The south Aegean active volcanic arc, present knowledge and future perspectives, edited by: Fytikas, M. and Vougioukalakis, G. E., Dev. Volcanol., 7, 65–111, ISBN 0-444-52046-5, 2005.
- Higgins, O., Sheldrake, T., and Caricchi, L.: Machine learning thermobarometry and chemometry using amphibole and clinopyroxene: a window into the roots of an arc volcano (Mount Liamuiga, Saint Kitts), Contrib. Mineral. Petr., 177, 10, https://doi.org/10.1007/s00410-021-01874-6, 2022.
- Humphreys, M. C. S., Blundy, J., and Sparks, R. S. J.: Magma Evolution and Open-System Processes at Shiveluch Volcano: Insights from Phenocryst Zoning, J. Petrol., 47, 2303–2334, https://doi.org/10.1093/petrology/egl045, 2006.
- Humphreys, M. C. S., Christopher, T., and Hards, V.: Microlite transfer by disaggregation of mafic inclusions following magma mixing at Soufrière Hills volcano, Montserrat, Contrib. Mineral. Petr., 157, 609–624, 2009.
- Huppert, H. E.: Phase changes following the initiation of a hot turbulent flow over a cold solid surface, J. Fluid Mech., 198, 293–319, https://doi.org/10.1017/S0022112089000145, 1989.
- Hutchison, W., Fusillo, R., Pyle, D. M., Mather, T. A., Blundy, J. D., Biggs, J., Yirgu, G., Choen, E. B., Brooker, R. A., Barfod, D.

- N., and Calvert, A. T.: A pulse of mid-Pleistocene rift volcanism in Ethiopia at the dawn of modern humans, Nat. Commun., 7, 13192, https://doi.org/10.1038/ncomms13192, 2016.
- Kennedy, B. M., Holohan, E. P., Stix, J., Gravley, D. M., Davidson, J. R. J., and Cole, J. W.: Magma plumbing beneath collapse caldera volcanic systems, Earth. Sci. Rev., 177, 404–424, https://doi.org/10.1016/j.earscirev.2017.12.002, 2018.
- Klaver, M., Matveev, S., Berndt, J., Lissenberg, C. J., and Vroon, P. Z.: A mineral and cumulate perspective to magma differentiation at Nisyros volcano, Aegean arc, Contrib. Mineral. Petr., 172, 95, https://doi.org/10.1007/s00410-017-1414-5, 2017.
- Klaver, M., Blundy, J. D., and Vroon, P. Z.: Generation of arc rhyodacites through cumulate-melt reactions in a deep crustal hot zone: Evidence from Nisyros volcano, Earth Planet. Sc. Lett., 497, 169–180, https://doi.org/10.1016/j.epsl.2018.06.019, 2018.
- Krawczynski, M., Grove, T. L., and Beherens, H.: Amphibole stability in primitive arc magmas: effects of temperature, H₂O content, and oxygen fugacity, Contrib. Mineral Petr., 164, 317–339, doi.10.1007/s00410-012-0740-x, 2012.
- Laumonier, M., Scaillet, M., Pichavant, M., Champallier, R., Andujar, J., and Arbaret, L.: On the conditions of magma mixing and its bearing on andesite production in the crust, Nat. Commun., 5, 5607, https://doi.org/10.1038/ncomms6607, 2014.
- Laumonier, M., Karakas, O., Bachmann, O., Gaillard, F., Lukacs, R., Seghedi, I., Menand, T., and Harangi, S.: Evidence for a persistent magma reservoir with large melt content beneath an apparently extinct volcano, Earth Planet. Sc. Lett., 521, 79–90, 2019.
- Landi, P., La Felice, S., Petrelli, M., Vezzoli, L. M., and Principe, C.: Deciphering textural and chemical zoning of K-feldspar megacrysts from Mt. Amiata Volcano (Southern Tuscany, Italy): Insights into the petrogenesis and abnormal crystal growth, Lithos, 324–325, 569–583, https://doi.org/10.1016/j.lithos.2018.11.032, 2019.
- Larsen, J. F.: Rhyodacite magma storage conditions prior to the 3430 yBP caldera-forming eruption of Aniakchak volcano, Alaska, Contrib. Mineral. Petr., 152, 523–540, https://doi.org/10.1007/s00410-006-0121-4, 2006.
- Lepage, L. D.: ILMAT: an Excel worksheet for ilmenite-magnetite geothermometry and geobarometry, Comput. Geosci., 29, 673– 678, 2003.
- Limburg, E. M. and Varekamp, J. C.: Young pumice deposits on Nisyros, Greece, Bull. Volcanol., 54, 68–77, 1991.
- Lindsley, D. H.: Pyroxene thermometry, Am. Mineral., 68, 477–493, 1983.
- Liu, Y., Zhang, Y., and Behrens, H.: Solubility of H_2O in rhyolitic melts at low pressures and a new empirical model for mixed H_2O – CO_2 solubility in rhyolitic melts, J. Volcanol. Geoth. Res., 143, 219–235, 2005.
- Locher, V., Popa, R. G., Guillong, M., and Bachmann, O.: Insights into caldera cycles obtained form the eruption ages and chemistry of the youngest products of Nisyros volcano, South Aegean Arc, J. Volcanol. Geotherm. Res., 460, 108281, https://doi.org/10.1016/j.jvolgeores.2025.108281, 2025.
- Locock, A. J.: An Excels preadsheet to classify chemical analyses of amphiboles following the IMA 2012 recommendations, Comput. Geosci., 62, 1–11, https://doi.org/10.1016/j.cageo.2013.09.011, 2014.

- Longchamp, C., Skopelitis, A., Bonadonna, C., and Bachmann, O.: Characterization of tephra deposits with limited exposure: the example of the two largest explosive eruptions at Nisyros volcano (Greece), Bull. Volcanol., 73, 1337–1352, 2011.
- Maestrelli, D., Corti, G., Bonini, M., Keir, D., Facincani, P., Vannucchi, P., Del Ventisette, C., Montanari, D., and Sani, F.: Fault reactivation and growth at rift-related calderas, Earth Planet. Sc. Lett., 636, 118700, https://doi.org/10.1016/j.epsl.2024.118700, 2024
- Margari, V., Pyle, D. M., Bryant, C., and Gibbard, P. L.: Mediterranean tephra stratigraphy revisited: results from a long terrestrial sequence on Lesvos Island, Greece, J. Volcanol. Geotherm. Res., 163, 34–54, 2007.
- Mastroianni, F., Braschi, E., Di Salvo, S., Casalini, M., Agostini, S., Vougioukalakis, G. E., and Francalanci, L.: Data on unveiling the occurrence of transient, multi-contaminated mafic magmas inside a rhyolitic reservoir feeding an explosive eruption (Nisyros, Greece), Data in Brief, 42, 108077, https://doi.org/10.1016/j.dib.2022.108077, 2022.
- Petrelli, M., Caricchi, L., and Perugini, D.: Machine learning thermo-barometry: Application to clinopyroxene-bearing magmas, J. Geophys. Res.-Sol. Ea., 125, e2020JB020130, https://doi.org/10.1029/2020JB020130, 2020.
- Petrone, C. M., Braschi, E., Francalanci, L., Casalini, M., and Tommasini, S.: Rapid mixing and short storage timescale in the magma dynamics of a steady-state volcano, Earth Planet. Sc. Lett., 492, 206–221, 2018.
- Pichavant, M. and Macdonald, R.: Crystallization of primitive basaltic magmas at crustal pressures and genesis of the calcalkaline igneous suite: experimental evidence from St Vincent, Lesser Antilles arc, Contrib. Mineral. Petr., 154, 535–558, 2007.
- Popa, R.-G., Walter, T. R., Richter, N., Gestrich, M., Klügel, A., Perugini, D., and Fiorentino, A.: A connection between magma chamber processes and eruptive styles revealed at Nisyros-Yali volcano (Greece), J. Volcanol. Geotherm. Res., 387, 106666, https://doi.org/10.1016/j.jvolgeores.2019.106666, 2019.
- Popa, R.-G., Guillong, M., Bachmann, O., Szymanowski, D., and Ellis, B.: U-Th zircon dating reveals a correlation between eruptive styles and repose periods at the Nisyros-Yali volcanic area, Greece, Chem. Geol., 555, 119830, https://doi.org/10.1016/j.chemgeo.2020.119830, 2020.
- Popa, R. G., Bachmann, O., and Huber, C.: Explosive or effusive style of volcanic eruption determined by magma storage conditions, Nat. Geosci., 14, 781–786, https://doi.org/10.1038/s41561-021-00827-9, 2021a.
- Popa, R.-G., Tollan, P., Bachmann, O., Schenker, V., Ellis, B., and Allaz, J. M.: Water exsolution in the magma chamber favors effusive eruptions: Application of Cl-F partitioning behavior at the Nisyros-Yali volcanic area, Chem. Geol., 570, 120170, https://doi.org/10.1016/j.chemgeo.2021.120170, 2021b.
- Putirka, K. D.: Thermometers and barometers for volcanic systems, Rev. Mineral. Geochem., 69, 61–120, https://doi.org/10.2138/rmg.2008.69.3, 2008.
- Putirka, K. D.: Amphibole thermometers and barometers for igneous systems and some implications for eruption mechanisms of felsic magmas at arc volcanoes, Am. Mineral., 101, 841–858, https://doi.org/10.2138/am-2016-5506, 2016.

- Ridolfi, F.: Amp-TB2: an updated model for calcic amphibole thermobarometry, Minerals, 11, 324, https://doi.org/10.3390/min11030324, 2021.
- Ruprecht, P. and Wörner, G.: Variable regimes in magma systems documented in plagioclase zoning patterns: El Misti stratovolcano and Andahua monogenetic cones, J. Volcanol. Geotherm. Res., 165, 142–162, https://doi.org/10.1016/j.jvolgeores.2007.06.002, 2007.
- Ruprecht, P., Simon, A. C., and Fiege, A.: The survival of mafic magmatic enclaves and the timing of magma recharge, Geophys. Res. Lett., 47, e2020GL087186, https://doi.org/10.1029/2020GL087186, 2020.
- Seymour, K. and Vlassopoulos, D.: Magma mixing at Nisyros volcano, as inferred from incompatible trace-element systematics, J. Volcanol. Geotherm. Res., 50, 273–299, https://doi.org/10.1016/0377-0273(92)90097-W, 1992.
- Sisson, T. W. and Grove, T. L.: Experimental investigations of the role of H₂O in calcalkaline differentiation and subduction zone magmatism, Contrib. Mineral. Petr., 113, 143–166, 1993.
- Smith, P. E., York, D., Chen, Y., and Evensen, N. M.: Single crystal ⁴⁰ Ar/³⁹ Ar dating of a Late Quaternary paroxysm on Kos, Greece: concordance of terrestrial and marine ages, Geophys. Res. Lett., 23, 3047–3050, 1996.
- Sparks, R. S. J., Blundy, J. D., Cashman, K. V., Jackson, M., Rust, A. C., and Wilson, C.: Large silicic magma bodies and very large magnitude explosive eruptions, Bull. Volcanol., 84, https://doi.org/10.1007/s00445-021-01510-y, 2022.
- Sparks, R. S. J., Cashman, K. V., Blundy, J. D., and Humphreys, M. C. S.: Source reservoir controls on the size, frequency, and composition of volcanic super-eruptions, Sci. Adv., 10, eadd1595, https://doi.org/10.1126/sciadv.add1595, 2024.
- Stormer, J. C.: The effects of recalculation on estimates of temperature and oxygen fugacity from analyses of multicomponent irontitanium oxides, Am. Mineral., 68, 586–594, 1983.

- Szymanowski, D., Wotzlaw, J. F., Ellis, B. S., Bachmann, O., Guillong, M., and von Quadt, A.: Protracted near-solidus storage and pre-eruptive rejuvenation of large magma reservoirs, Nat. Geosci., 10, 777–782, 2017.
- Tibaldi, A., Pasquare, F. A., Papanikolaou, D., and Nomikou, P.: Tectonics of Nisyros Island, Greece, by field and offshore data, and analogue modelling, J. Struct. Geol., 30, 1489–1506, https://doi.org/10.1016/j.jsg.2008.08.003, 2008.
- Vanderkluysen, L., Volentik, A. C. M., Principe, C., Hunziker, J. C., and Hernandez, J.: Nisyros' volcanic evolution: the growth of a strato-volcano, in: The geology, geochemistry and evolution of Nisyros Volcano (Greece), edited by: Hunziker, J. C. and Marini, L., Mémoires de Géologie (Lausanne), No. 44, 100–104, ISSN 1015-3578, 2005.
- Varekamp, J. C.: Some remarks on volcanic vent evolution during Plinian eruptions, J. Volcanol. Geotherm. Res., 54, 309–318, https://doi.org/10.1016/0377-0273(93)90069-4, 1993.
- Volentik, A., Vanderkluysen, L., and Principe, C.: Stratigraphy of the caldera walls of Nisyros volcano, Greece, Eclogae Geol. Helv., 95, 223–235, 2002.
- Volentik, A., Principe, C., Vanderkluysen, L., and Hunziker, J. C.: Explanatory notes on the "Geological Map of Nisyros Volcano (Greece)", in: The Geology, Geochemistry and Evolution of Nisyros Volcano (Greece), Implications for the Volcanic Hazards, edited by: Hunziker, J. C. and Marini, L., Mémoires de géologie (Lausanne), 44, 26–66, 2005.
- Vougioukalakis, G.: Volcanic stratigraphy and evolution of Nisyros island, Bulletin of Geological Society, Greece, Athens, XXVI-II/2, 239–258, 1993.
- Waters, L. E. and Lange, R. A.: An updated calibration of the plagioclase-liquid hygrometer-thermometer applicable to basalts through rhyolites, Am. Mineral., 100, 2172–2184, https://doi.org/10.2138/am-2015-5232, 2015.
- Wyers, G. P. and Barton, M.: Polybaric evolution of calc-alkaline magmas from Nisyros, Southeastern Hellenic Arc, Greece, J. Petrol., 30, 1–37, 1989.